Exploring Fiber-Reinforced Polymer Concrete for Accelerated Bridge Construction Applications

Carolyn Donohoe

A thesis

submitted in partial fulfillment of the

requirements for a degree of

Master of Science

University of Washington

2022

Committee:

Travis Thonstad

John Stanton

Paolo Calvi

Program Authorized to Offer Degree:

Civil and Environmental Engineering

University of Washington

Abstract

Exploring Fiber-Reinforced Polymer Concrete for Accelerated Bridge Construction Applications

Carolyn Donohoe

Chair of the Supervisory Committee:

Travis Thonstad

Civil and Environmental Engineering

The use of prefabricated superstructure elements in bridge construction reduces on-site construction time, improves work-zone safety, and can reduce overall project costs. For prefabricated elements to be used efficiently for accelerated bridge construction (ABC), the precast components, such as deck panels or decked-bulb tees, must be connected quickly on-site, ideally using as little additional material as possible.

The use of fiber-reinforced polymer concrete (FRPC) was explored as a closure pour material for bridges to connect adjacent precast superstructure elements. Polymer concretes have been used successfully as a non-structural overlay material in transportation systems for many decades. With the addition of fibers, FRPC displays levels of two critical characteristics, bond and tension strength, that are comparable to other alternatives, such as ultra-high performance concrete (UHPC). While UHPC may still provide the best solution in many instances, FRPC has the advantage of requiring shorter closure windows (approximately 4 hours versus 72 hours for

UHPC) due to the very rapid strength gain of the polymer, which could be ideal for overnight construction or rehabilitation projects.

The bond and mechanical properties of FRPC were determined at several temperatures, spanning the range of typical service conditions in western Washington State. Tests were completed measuring the compressive, flexural, and bond strength of FRPC. Then, a central composite rotatable experimental design was utilized to explore the impact of splice length, side cover, bar size, and temperature on bar stress in non-contact splice specimens. The test setup was similar to that completed by the Federal Highway Administration (FHWA) with UHPC.

The results of the testing program indicate that FRPC exhibits significant variation in mechanical properties with temperature, roughly -0.6 %/°F; the development of early compressive, flexure, and bond strengths were very similar, reaching roughly 70% of their 7-day values in 4 hours; and peak bar stresses in non-contact lap splices embedded in FRPC were comparable to UHPC for the embedded lengths tested. Based on the testing results, example joint configurations for connecting precast superstructure elements were developed, enabling the comparison of FRPC with alternative closure pour materials for future ABC projects.

TABLE OF CONTENTS

List of Figures iii
List of Tables v
List of Acronyms vi
Chapter 1. Introduction 1
1.1. Objectives 7
1.2. Organization of Thesis 8
Chapter 2. Background 10
2.1. Binder 10
2.2. Mixture Design 13
2.3. Mechanical Properties 14
2.3.1. Temperature Effects 19
2.4. Reinforcement 25
Chapter 3. Material Characterization 30
3.1. Commercial Products 30
3.2. Material Components 31
3.3. Mixing Procedure 32
3.4. Specimen Fabrication 33
3.5. Testing Setup 34
3.6. Compressive Strength of 7-Day Control Cylinders 37
3.7. Temperature Rise During Hardening 38
3.8. Strength Gain Over Time 39
3.9. Influence of Testing Temperature 43
Chapter 4. Non-Contact Splice Testing Program 48
4.1. Design of Experiments 48
4.2. Concrete 53
4.3. Deformed Bar Reinforcement 54

4.4. Polymer Concrete 55
4.5. Construction Sequence 56
4.6. Temperature During Conditioning 57
4.7. Instrumentation 58
4.8. Test Procedure 60
4.9. Temperature During Testing 61
Chapter 5. Results 62
5.1. Influence of Primer 63
5.2. Influence of Temperature, Splice length, and Bar Cover 65
5.2.1. Batch-to-Batch Variability 67
5.2.2. Stress-Slip Behavior 68
5.2.3. Maximum Bar Stress 72
Chapter 6. Design Recommendations 78
6.1. Closure Joint Geometry 78
Chapter 7. Summary, Conclusions, and Recommendations 84
7.1. Summary 84
7.2. Conclusions 85
7.3. Recommendations for Further Research 86
References 87

LIST OF FIGURES

Figure 1-1. (a) Precast concrete girder closure joint - plan and section, adapted from Peruchini (2017), (b) precast deck panel closure joint - section and detail 2
Figure 1-2. Timeline of UHPC usage in bridge construction in (a) the United States, (b) Canada. Data from Haber et al. (2018) 4
Figure 1-3. (a) Wheel path PPC inlay, (b) PPC overlay with diamond grinding (Anderson et al. 2013) 6
Figure 2-1. Schematic of polymerization and cross-linking 11
Figure 2-2. Compressive stress-strain behavior of polymer concretes at room temperature 18
Figure 2-3. Previous studies investigating the influence of temperature on compressive strength 20
Figure 3-1. (a) Mixing of MEKP and HCSC resin with a squirrel cage mixer, (b) Resin mixture being transferred from mixing bucket to drum mixing, (c) Adding the pre-packaged aggregate and fiber blend to the drum mixer, (d) HCSC mix turning in drum mixer, (e) HCSC placed in cylinder molds before finishing 33
Figure 3-2. Diagrams and test setup for (a/d) compressive strength, (b/e) modulus of rupture, (c/f) bond pullout 35
Figure 3-3. (a) Debonded section of the specimen, (b) test diagram, (c) testing setup 36
Figure 3-4. Histogram of 7-day compressive cylinder strengths 38
Figure 3-5. Temperature of specimens during curing 39
Figure 3-6. Beam stiffness and modulus of elasticity as a function of time after mixing 40
Figure 3-7. Stress-back end slip for bond pullout testing as a function of time after mixing 41
Figure 3-8. Strength (compression, flexure, bond, normalized) as a function time after mixing. 43
Figure 3-9. Beam stiffness and modulus of elasticity as a function of test temperature 44
Figure 3-10. Stress-back end slip for bond pullout testing as a function of testing temperature.. 45
Figure 3-11. Strength (compression, flexure, bond, normalized) as a function of test temperature 46
Figure 3-12. Linear Strength Regression (compression, flexure, bond, normalized) as a function of test temperature 47
Figure 4-1. Loading setup by Yuan and Graybeal (2014) 48

Figure 4-2. (a) Elevation and section view of non-contact splice specimen,
(b) diagram of testing setup 49
Figure 4-3. Tensile stress-strain response of epoxy-coated reinforcing bars 54
Figure 4-4. Non-contact splice specimen casting procedure:
(a) cementitious concrete formwork, (b) cast cementitious concrete,
(c) exposed aggregate finish, (d) HCSC formwork 57
Figure 4-5. Temperature of non-contact splice specimens during curing 58
Figure 4-6. (a) LVDT placement on reinforcement, (b) embedded thermocouples 59
Figure 4-7. Non-contact splice testing setup 60
Figure 4-8. Internal and surface specimen temperature for similar specimens 61
Figure 5-1. (a) Elevation view of splitting failure, 2-10, (b) Splitting at top of HCSC, 2-10 63
Figure 5-2. Main effects of usage of HMWM primer 65
Figure 5-3. (a) Elevation view of bar fracture, 1-02, (b) Rebar at top of HCSC, 1-02,
(c) Bar fracture and top of HCSC, 1-04 66
Figure 5-4. (a) Elevation view of pullout failure, 2-04, (b) Pullout at top of HCSC, 2-04 66
Figure 5-5. Stress-front end displacement for temperature star points and center points 69
Figure 5-6. Stress-front end displacement for splice length star points and center points 70
Figure 5-7. Stress-front end displacement for side cover star points and center points 70
Figure 5-8. Stress- front end displacement for bar size star points and center points 71
Figure 5-9. Comparison of normalized splice length and bar stress 73
Figure 5-10. Main effects of CCD analysis 75
Figure 5-11. Interaction diagram of CCD analysis 77
Figure 6-1. Conventional concrete closure joint per AASHTO specifications
(Garber and Shahrokhinasab 2019) 79
Figure 6-2. UHPC Recommended joint geometry (Garber and Shahrokhinasab 2019) 80
Figure 6-3. Bar stress for varying temperatures and bar sizes 81

LIST OF TABLES

Table 2-1. Mechanical properties from previous polymer concrete studies 16
Table 2-2. Previous studies investigating the effect of temperature 22
Table 2-3. Previous studies investigating the influence of fibers 27
Table 3-1. Summary of PPC and HCSC Mechanical Properties 30
Table 3-2. HCSC mix design 31
Table 3-3. HMWM primer mix design, by volume 31
Table 3-4. Normalized compressive strength and working time for various accelerator volumes 32
Table 3-5. Mechanical property specimen catalog 37
Table 3-6. Beam stiffness and modulus of elasticity as a function of time after mixing 40
Table 3-7. Beam stiffness and modulus of elasticity as a function of test temperature 44
Table 4-1. Summary of test parameters 50
Table 4-2. Non-contact splice experimental matrix 52
Table 4-3. Scoping study experimental matrix 53
Table 4-4. Cementitious concrete compressive strengths 53
Table 4-5. Properties of reinforcing steel 55
Table 4-6. HCSC compressive strengths 56
Table 4-7. Average surface and internal temperature during testing 61
Table 5-1. Summary of experimental testing results 62
Table 5-2. Percent change in bar stress due to HMWM primer usage 64
Table 5-3. Bar stress at failure for repeated center point specimens 67
Table 5-4. Analysis of Variance Results 74

LIST OF ACRONYMS

AASHTO	American Association of State Highway and Transportation Officials
ABC	Accelerated bridge construction
ACI	American Concrete Institute
ANOVA	Analysis of variance
ASTM	American Society for Testing and Materials
CHP	Cumene hydro peroxide
FHWA	Federal Highway Administration
FRPC	Fiber-reinforced polymer concrete
HCSC	Hybrid Composite Synthetic Concrete
HMWM	High molecular weight methacrylate
LRFD	Load and resistance factor design
LVDT	Linear variable differential transformer
MDO	Medium-density overlay
MEKP	Methyl ethyl ketone peroxide
MMA	Methyl methacrylate
PC	Polymer concrete
PMMA	Polymethyl methacrylate
PPC	Polyester polymer concrete
RSM	Response surface methodology
UHPC	Ultra-high performance concrete

CHAPTER 1. INTRODUCTION

The new construction and repair of transportation structures can be costly, affect the safety of workers, and reduce public usability due to the large duration in which construction may occur. The concrete structural elements can be cast in place with formwork, pouring of material, resulting in all, or a majority of the structures components being built at the construction site. However, this approach can cause increases in construction time, weather-related delays, traffic impacts, negatively impact the quality of construction, and ultimately increase construction costs. Accelerated bridge construction (ABC) shifts the procurement and construction of elements to provide an alternate method of bridge construction. By constructing elements offsite and then transporting and installing them onsite, ABC improves the total project timeline by allowing parallel construction and reducing traffic delays caused by extended time of infrastructure closure.

The use of precast concrete superstructure elements is a popular strategy for ABC and rehabilitation projects. Once delivered to the site, adjacent precast superstructure elements must be connected at closure joints or keyways. These joints can be “longitudinal”, i.e., parallel to the direction of traffic, where a bridge span comprises multiple adjacent decked girders, as shown in Figure 1-1a. The joints can also be “transverse”, or perpendicular to the direction of traffic when full-width deck panels are used to form the bridge superstructures, as shown in Figure 1-1b. These joints are crucial for providing a continuous load path between elements and throughout the structure.

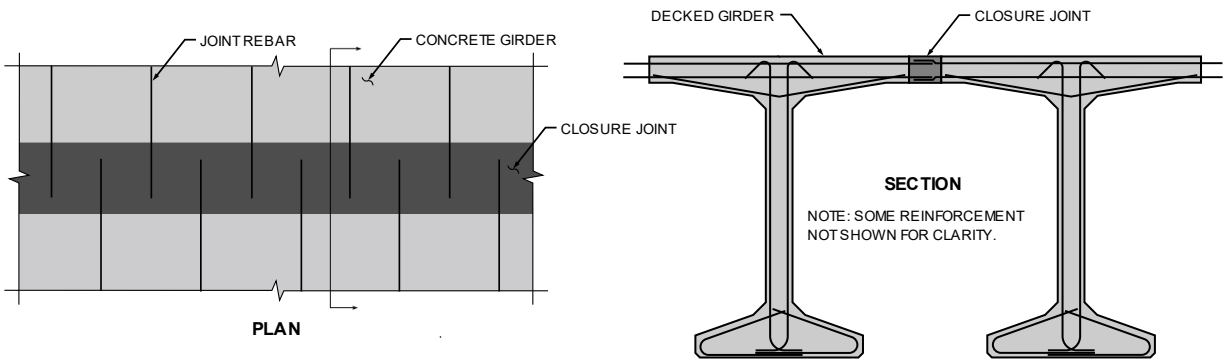

(a)

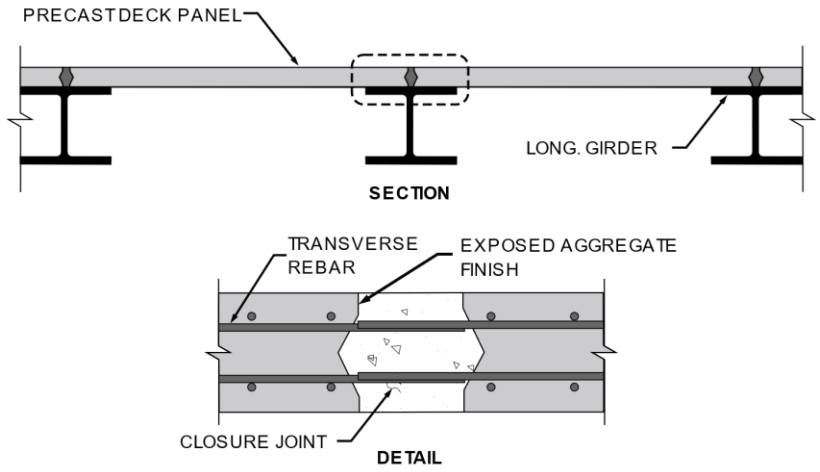

(b)

Figure 1-1. (a) Precast concrete girder closure joint - plan and section, adapted from Peruchini (2017), (b) precast deck panel closure joint - section and detail

To complete the superstructure, the closure joints are filled with a field-cast material that creates continuity between the precast concrete elements and splices steel reinforcement protruding from the precast members into the joints. These connections are also integral for the development of the bridge loading path between structural elements. The American Association of State Highway and Transportation Officials (AASHTO) provides specifications for highways and construction in the United States. The AASHTO specifications require that the concrete deck be "sufficiently connected to act as a unit." (AASHTO LRFD Section 4.6) AASHTO also specified the minimum required lengths for splices and development lengths for reinforcement. These requirements help

ensure that there is a continuous load path between the different structural elements during the life of the structure.

The geometry of the closure joints, the speed at which the connections can be completed, the curing time required before the bridge can be opened to traffic, and the cost of the system are all dependent on the material that is used to fill the gaps between precast elements. The closure joint material must possess strength and durability equal to or greater than the adjacent concrete and must be capable of transferring the tensile forces between reinforcement from adjacent precast elements. The major advantage is that precast concrete elements can be fabricated before, or in parallel with, on-site activities, thus expediting project delivery. Additionally, because precast concrete components are constructed in specialized facilities under controlled conditions, component quality is often improved over cast-in-place methods.

Presently, the most common material used in closure joints is ultra-high performance concrete (UHPC). UHPC is a cementitious, fiber-reinforced, composite material with mechanical and durability properties far exceeding those of conventional concrete. UHPC has been commercially available for more than a decade in the United States and Canada, with usage rapidly increasing as additional research has been performed and bridge designers and owners understand its advantages. Figure 1-2a and Figure 1-2b show the increase in the use of UHPC in bridge construction over the last decade.

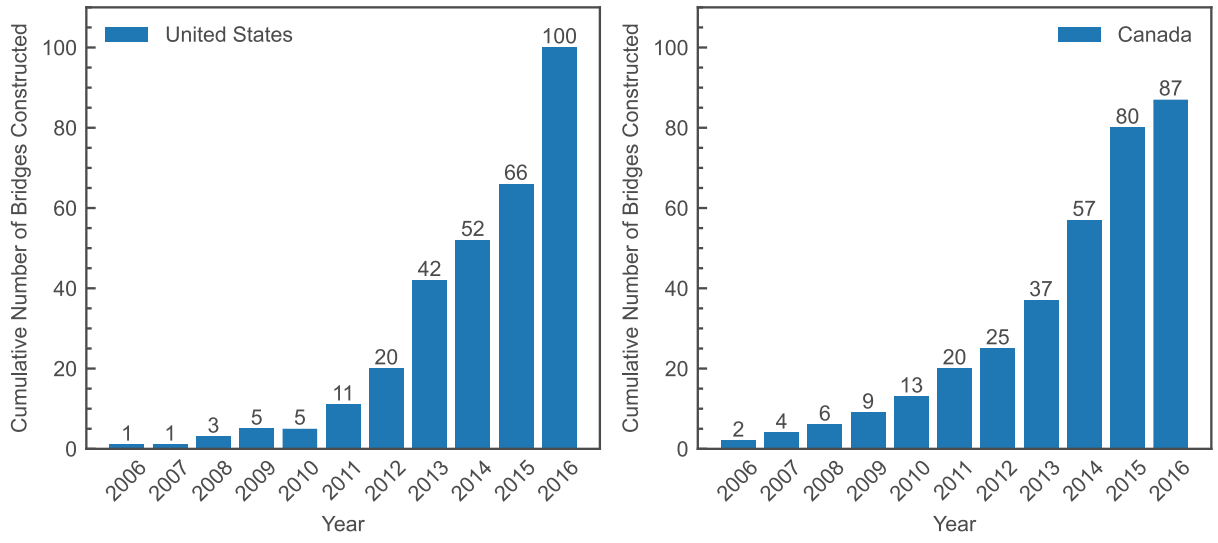

(a) (b)

Figure 1-2. Timeline of UHPC usage in bridge construction in (a) the United States, (b) Canada. Data from Haber et al. (2018)

The excellent tensile and bond strengths of UHPC make it ideal for joining prefabricated elements together, reducing the required splice length between reinforcement, and thus the joint size between components. The properties and capabilities of specific UHPC mixes have been extensively studied, most prominently at the Federal Highway Administration (FHWA) and Accelerated Bridge Construction University Transportation Center (e.g., Graybeal 2006, Graybeal 2014, Haber et al. 2018, Shahrokhinasab and Garber 2021), and are relatively well understood. However, most ABC and other construction projects rely on proprietary UHPC materials, at the contractor's request. This provides a lower risk to the contractor as the material supplier often comes to the site and takes responsibility for the batching and mixing but increases the cost of the closure pour. While UHPC may still provide the best solution in many instances, alternative materials exist with similar mechanical properties that may prove advantageous in certain applications.

Similar to traditional cementitious concretes, polymer concretes (PCs) are composed of a mix of aggregates and resin or monomers. In contrast with UHPC, PCs do not contain hydrated cement paste. The material hardens and gains its strength by cross-linking. Polymer concretes can be tailored to have a variety of properties depending on the formulation of the polymer used, including rapid curing at ambient temperatures, high tensile and flexural strength, good chemical resistance, and good adhesion to most surfaces (ACI 2019). Fiber-reinforced polymer concretes (FRPC) are polymer concretes with the addition of fibers. FRPCs are a potential alternative material to UHPC in the ABC field.

Polymer concrete was first used in commercial applications within the United States in the 1950s (ACI 2019). First used in the production of synthetic materials and cladding in architectural fields, PCs were later used as an overlay material for structural applications (Fowler 1999, Maas 1997). Initially, the broom-and-seed method was used but was not very effective due to permeability and durability issues (Fowler and Whitney 2012). Improvements to the material composition in the 1960s and 1970s resulted in the usage of epoxy, polyester styrene, or methyl methacrylate in the PC mix design. These developments were an improvement from the original mix design and construction technique but still resulted in problems like delamination and reduced performance when compared to current designs. Additional and substantial improvements were made to both the PC mixtures and overlay construction practices that improved performance (Maas 2003, Fowler and Whitney 2012). Premixed polyester polymer concrete (premixing of aggregates and resin before placement) was developed in the late 1970s and soon became the standard for placement of overlays. Figure 1-3 shows the use of polyester polymer concrete (PPC) as an inlay and overlay material in Spokane, Washington. Multiple state's department of transportation utilize PC overlays, most notably California and New York. PC overlays are durable and provide high

protection against moisture and chloride ions from deicing salts (Maas 2003). They are also resistant to cracking and delamination and have service life of up to 20 years, longer than other traditional overlays (Sprinkel 2003).

(a) (b)

Figure 1-3. (a) Wheel path PPC inlay, (b) PPC overlay with diamond grinding (Anderson et al. 2013)

Despite being used as an overlay material for over 40 years and the promising experimental results, there are few examples of PC used for closure joints or other full-depth repairs. Previous studies investigating PCs for closure joints between precast deck panels found that specimens constructed with PC closure joints had similar strengths and lower initial stiffnesses than those constructed with UHPC (Moustafa et al. 2019). Mantawy et al. (2019), (FIU) studied the bond and splice characteristics of a polymethyl methacrylate polymer concrete and found that the bond strength was higher, and the splice length was shorter, for the specimens containing PC in comparison with those containing UHPC.

The addition of fibers to PCs leads to improved properties that could lead to smaller and simpler joint geometries when compared with UHPC or polymer concretes without fibers. There is the potential for smaller closure windows than when using UHPCs due to the faster strength gain of

the polymer. This hesitancy in the use of FRPC closure joints by bridge owners and agencies is largely due to the sparsity of experimental data and the lack of specific design guidance that accounts for the unique mechanical properties of FRPC in these applications. Further experimental investigation into the FRPC's mechanical and bond properties is crucial to understanding its capabilities in structural and ABC usage.

1.1. OBJECTIVES

The primary objectives of this research are to:

- Characterize the material properties of the FRPC at multiple temperatures and ages. In order to be used as a closure pour material, the mechanical properties of FRPC at early ages and various service temperatures must be well understood. This project tested FRPC at 10 different points throughout the curing process and at four different service temperatures once fully cured. These tests were performed for compressive, flexural, and bond strength.
- Characterize the splice performance of deformed bars embedded in FRPC at multiple temperatures. The width of the closure joint between elements is dependent on the bond strength of the reinforcement to the closure pour material. The development and non-contact splice behavior of bars in FRPC must be characterized for a range of potential design parameters. This was done by testing 30 non-contact splice specimens with varying bar size, test temperature, splice length, and side cover. The results were then analyzed to understand the individual impact of each parameter on the bond strength of an embedded bar.

- Develop preliminary design recommendations for the use of FRPC in ABC applications. The cost of using FRPC must not be prohibitive in comparison with other alternatives. Using the experimental results, design guidance and example joint configurations were developed to provide efficient, cost-effective recommendations to the designer and contractor for best use of FRPC as a closure joint material.

1.2. ORGANIZATION OF THESIS

The report is organized as follows:

- Chapter 2: Background
    - A breakdown of the mixture design for polymer concretes and a collection of past experiments conducted on polymer concrete with varying mix designs and their associated mechanical properties
- Chapter 3: Material Characterization
    - The mix design, mixing and casting procedure, and testing plan for compression, flexural beam, and bond pullout testing. Tests include strength gain over time and different testing temperatures for each type of test.
- Chapter 4: Non-Contact Splice Testing Program
    - An explanation of the experimental designs, specimen geometry, and specimen parameters used for non-contact splice specimen testing.
    - A breakdown of the construction sequence, specimen monitoring, and test procedure for the testing of the influence of primer, geometric, and temperature parameters.
- Chapter 5: Results
    - Test results are reported for each specimen through tables, plots, and photos.

- Discussion and analysis of results based on statistical analysis from the design of the experiment. The analysis focuses on the influence of temperature, splice length, side cover, and bar size

- Chapter 6: Design Recommendations
  - Recommendations for longitudinal joint geometry are proposed with guidance for required splice length and side cover.
- Chapter 7: Summary, Conclusions, and Recommendations
  - A summary of the completed work, conclusions drawn based on the results of the study, and recommendations for future work.

CHAPTER 2. BACKGROUND

Polymer concrete has been used in a variety of commercial applications such as floor drains, utility drains, etc. since the 1970s (ACI 2019), with its first uses in the United States in 1958 as building cladding (Fowler 1999). A variety of commercially produced PC products are available throughout the US and are typically provided in prepackaged bags and buckets with each mix component. Kwik Bond's polyester polymer concrete, Transpo's T-17 methyl methacrylate polymer concrete, Sika's Sikadur-32 epoxy polymer concrete, and others have been used for overlay systems, patching, and grouting (Kwik Bond Polymers 2020, Transpo Industries, Inc. n.d., Sika 2020). Unlike conventional concrete, which hardens through the hydration of cementitious materials, polymer concrete hardens via cross-linking of a monomer and polymer chain to form a connected, rigid network of crosslinked polymer chains. The mechanical and physical properties of polymer concrete vary based on the type and properties of the binder, the proportioning of aggregates and binder in the mixture, and the aggregate composition and type. The following sections describe each of these considerations in more detail.

2.1. BINDER

Cost, workability, stiffness, strength, and durability are all factors to consider when selecting the polymer binder for a particular application. Several binders are commonly used and commercially available for polymer concrete including epoxy, methacrylate, and polyester. Figure 2-1 summarizes the chemical process that occurs for a generic polyester-based polymer concrete, as an example. This particular pathway is popular in commercial applications because the two-part mixing process is simple for the installer, yet still allows adjustments for project and site-specific needs.

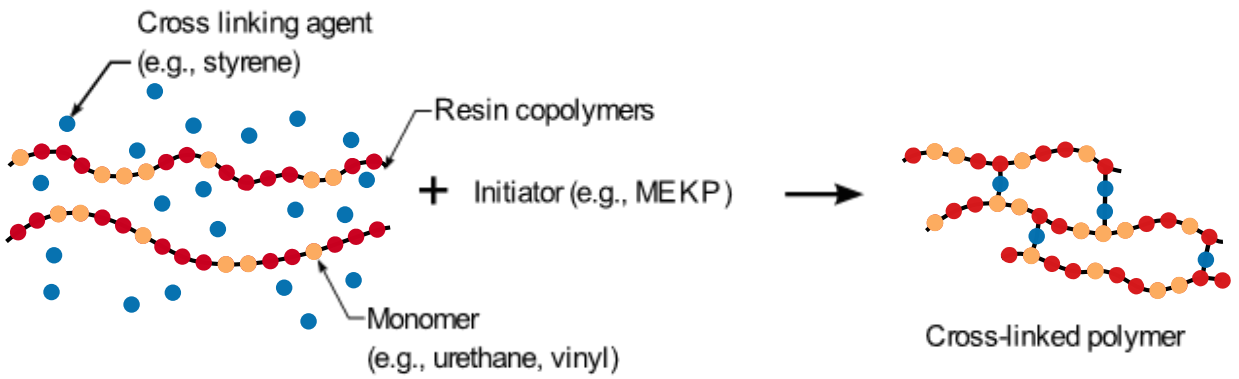

Figure 2-1. Schematic of polymerization and cross-linking

Monomers are small molecules that can bond to other monomers to form a polymer, a chain-like structure. Monomers can also exist by themselves, like styrene, which is a popular cross-linking agent. Promoters, sometimes called accelerators cause decomposition of the peroxide initiators and are used to modify the speed of the reaction. Initiators react with the promoter and result in the cross-linking reaction between cross-linking agent and the polymer chain (ACI 2019).

Prepackaged mixtures commonly have the resin copolymers in solution with the monomer cross-linking agent. When mixed with an initiator, the monomer and polymer chain form a cross-linked polymer with the monomer providing the link between the polymer chains. The cross-linking process is exothermic, increasing material temperature as it gels and hardens. This process creates a thermoset polymer, a polymer that will solidify when cured that can't be remolded due to the irreversible cross-linked bonds (ACI 2019). The cross-linked polymer physically binds with the aggregate, creating a cohesive material.

Cost, durability, adhesion to aggregate, ease of polymerization at room temperature, and vapor pressure all play a role in the selection of the monomer type (Hsu 1984). Most PC mixtures contain one or more monomers with a promoter and an initiator. The promoter-initiator pair is selected such that polymerization occurs at ambient conditions in 30 to 45 minutes. (Hsu 1984) Inhibitors and accelerators or promoters can be added to the resin to tune the work time before the mixture

reaches a gel point and workability is severely reduced. The usage of and amount of accelerator may be adjusted based on the ambient temperature, humidity, complexity of the pour, etc. Additives such as plasticizers, colorants, and flame retardants can also be included to modify the workability, mechanical properties, or appearance (Hsu 1984). The particular mix design can be adjusted for a range of working times, allowing PC's usage for a variety of applications.

Epoxy polymer concrete utilizes an epoxy resin as the binder. It is typically a two-component system, the epoxy resin and a curing agent or initiator. There is a large range of gel times and curing times, ranging from 3 minutes to 1 hour. The ratio of epoxy to hardener can also vary, which affects the mechanical and chemical properties. Epoxy polymer concrete is resistant to many chemicals, has low curing shrinkage, good adhesion properties, high tensile strengths, and excellent abrasion resistance (ACI 2019). The viscosity of epoxy resins can vary, with high viscosities having a putty-like and sticky finish and low viscosities having better workability. Both epoxy PC and polyester PC have properties that vary with the curing method and temperature.

Methacrylate polymer concrete broadly describes a form of PC that uses some form of methacrylate as the binder. The primary monomers used are methyl methacrylate (MMA) and high-molecular-weight methacrylate (HMWM). MMA is a highly volatile liquid with a strong odor and low viscosity. HMWM was developed to minimize the volatility of MMA, also reducing the odor and monomer loss via surface evaporation. For the polymerization process to begin in methacrylate PCs, an initiator and promoter must be used. In prepackaged systems, the promoter is mixed and packaged with the monomer with the initiator packaged separately. The ratio of initiator and promoter varies, providing a range of curing times and physical properties. This variety is tolerable in a methacrylate system, unlike epoxies where the ratio of components should not be adjusted to modify curing time. MMA systems typically have a working time between 15

and 60 minutes with rapid curing after the working period. The conditions required for curing have a large temperature range, including cold temperatures. Due to the excellent flow characteristics, MMA PCs are well suited for complex geometries and highly reinforced cross sections (ACI 2019).

Unsaturated PPC is made with polyester resin. Like methacrylate PCs, initiators and promoters are used as part of the polymerization process. An initiator, typically methyl ethyl ketone peroxide (MEKP) or a ketone peroxide blend, is added to the liquid monomer and promoter which causes a cross-linking reaction between the styrene monomer and the unsaturated polyester. This reaction results in a thermoset polymer – a strong and durable binder. Styrene monomers are comprised of a benzene ring and a vinyl functional group (Poillucci and Hansen 2013). They decrease the viscosity of the resin, providing increased workability. Cobalt naphthenate is sometimes also added as a catalyst to the polyester styrene mix. The specific type of polyester is based on the application conditions and the company's specific mix design.

2.2. MIXTURE DESIGN

Depending on the usage, the aggregates used in the mix design can vary from fines and sands to coarse aggregates. Polymer grout typically does not include aggregates, whereas polymer mortars include aggregate smaller than 1/4 in (ACI 2019). For large sections and overlays rounded river gravel up to 3/4 in. can be used. Well-graded aggregate mixtures are best used with low-viscosity binders, whereas gap-graded mixtures are best used with higher viscosities (Sprinkel 2003).

The morphology, cleanliness, and mechanical properties of the aggregate should be considered. Rounded surfaces of coarse aggregate and natural, clean sand aid in the workability of the mixtures, helping to reduce the amount of resin or binder required (Stevens and Guthrie 2021).

Silica sand, granite, river gravel, basalt, fly ash, calcium carbonate, and silica fume are typical options for use as fine aggregates and fine fillers in PC. Recycled materials such as rubber tire particles, cork granules, recycled concrete aggregate, silica fume, fly ash, etc. have been studied to help reduce the cost of PC and to reduce overall lifecycle waste. Commercial products include prepackaged proprietary blends of aggregate with or without fibers.

The presence of excess water in aggregate is known to reduce the mechanical strength of MMA PCs, with most specifications limiting the amount of moisture to one percent or less (Fowler et al. 1981). Therefore, aggregate used in PC should be dry and should not contain dirt, clay, asphalt, or other organic materials (Sprinkel 1997).

A multitude of laboratory studies researched various properties of PCs. With each study comes one and sometimes multiple mix designs. These studies have used a wide range of material ratios in their mix designs.

Based on aggregated results of previous studies on PC, aggregate content typically composes 75-90% of the total weight of the mixture and binder content is typically 10-15%. The remainder of the mixture is composed of microfillers, the initiator, and any accelerator used (Stevens and Guthrie 2021).

2.3. MECHANICAL PROPERTIES

The material properties of PCs are highly dependent on mix design, curing method, age, testing conditions, and procedures (Vipulanandan and Paul 1990). However, the variation in properties of test specimens from different batches within one mix design is typically small (ACI 2019). Table 2-1 summarizes material properties from various studies.

Compressive strength is often used as a design basis for structural concrete members and is an important field metric for the opening of structures. In general, polymer concretes can be designed with comparable or higher compressive strengths than conventional cementitious concrete at room temperature. Ranges in compressive strength are dependent on the binder, aggregate size, type, and gradation. A key characteristic of polymer concrete is its rapid strength gain, with studies showing 70-75% of final strength within 24 hours of curing at room temperature.

PCs typically have higher flexural and tensile strengths than cementitious concrete, with lower flexural moduli. The flexural strength of PC is highly dependent on the choice of polymer. Generally, highly cross-linked polymers result in higher flexural strengths. Hsu (1984), found that the modulus of rupture for PC varied linearly with the square root of compressive strength, similar to that of cementitious concrete.

Deformation of materials under load is dependent on the modulus of elasticity of the composite material. For PCs, the modulus of elasticity is highly dependent on the modulus of the polymer binder (ACI 2019). The high compressive strengths of PCs are achieved at much larger strains than cementitious concretes, and therefore polymer concretes tend to exhibit lower elastic moduli when compared with conventional cementitious concrete. Additionally, the mechanical properties of polymer concretes vary considerably with temperature, strain rate, and load duration.

Table 2-1. Mechanical properties from previous polymer concrete studies

Author	Resin	Compressive Strength (psi)	Modulus of Elasticity (ksi)	Modulus of Rupture (psi)	Bond Strength (psi)	Tensile Strength (psi)
Abdel-Fattah and El-Hawary 1999	Epoxy	% Resin by weight 9% = 5200, 12% = 5500, 15% = 3200	-	% Resin by weight 9% = 1300, 12% = 1500, 15% = 700	-	-
Abdel-Fattah and El-Hawary 1999	Epoxy	% Resin by weight 9% = 9100, 12% = 10400, 15% = 9300,		% Resin by weight 9% = 1900, 12% = 2200, 15% = 1800,	-	-
Abdel-Fattah and El-Hawary 1999	Polyester	% Resin by weight: 9% = 8000, 12% = 10400, 15% = 9100		% Resin by weight 9% = 1500, 12% = 2000, 15% = 1700		
Abokifa and Moustafa 2021	PMMA (Transpo T-17)	9000	2800	-	-	-
Al-Negheimish 1988	Epoxy	13600	3650	3100	-	-
Guedes et al. 2004	Epoxy	11900	1668	5600		-
Hassani Niaki et al. 2018	Epoxy	13600	-	5700	-	1700
Hong 2017	Epoxy	6000	-	3400	600	-
Hsu 1984	PMMA	9800	3240	2000	-	1300
Kwik Bond Polymers 2020a	Proprietary (HCSC)	10000	2500	2500	-	1500
Kwik Bond Polymers 2020b	Polyester (PPC 1121)	6000	1500	2000	700	800
Mani et al. 1987	Epoxy, polyester	Epoxy: 10400 Polyester: 6000	-	Epoxy: 3000 Polyester: 1800	-	-
Mantawy et al. 2019	PMMA	10500	-	-	-	1000

Mebarkia and Vipulanandan 1992	Polyester	10% PC, 6% fibers: 4800, 18% PC, 4% fibers: 12200	-	-	-	-
Oussama et al. 2012	Epoxy	% Resin by weight 6% = 3600, 9% = 5300, 13% = 12400, 16% = 13300		1800 2900 3400 3500	-	-
Reis 2005	Epoxy (Silicem Eposil 551), Masterflow 211, Emaco S88, Groutek S, Hagenpox	8700, 7400, 6500, 6500, 7200	1600	-	-	-
Ribeiro et al. 2004	Epoxy, polyester	-	-	Epoxy: 6100, Polyester: 3500	-	-
Sett and Vipulanandan 2004	Polyester	% Resin by weight 14% = 8000, 18% = 7600, 20% = 8600	-	-	-	14% = 1000
Toufigh et al. 2016	Epoxy (NITOBOND-EP, ML506-HA32, PR700-PH500)	9400 5200 5100	-	-	-	-
Vipulanandan and Mebarkia 1996	Polyester	-	-	2400	-	-
Vipulanandan and Paul 1990	Epoxy, polyester	Epoxy: 7400 Polyester: 7000	-	-		-
Wagner 2021	Proprietary (HCSC)	9000	2700	-	-	-

Figure 2-2 compares the compressive stress-strain behavior of several polymer concretes available in the literature. The stress-strain behavior for conventional concrete and UHPC are also included for reference.

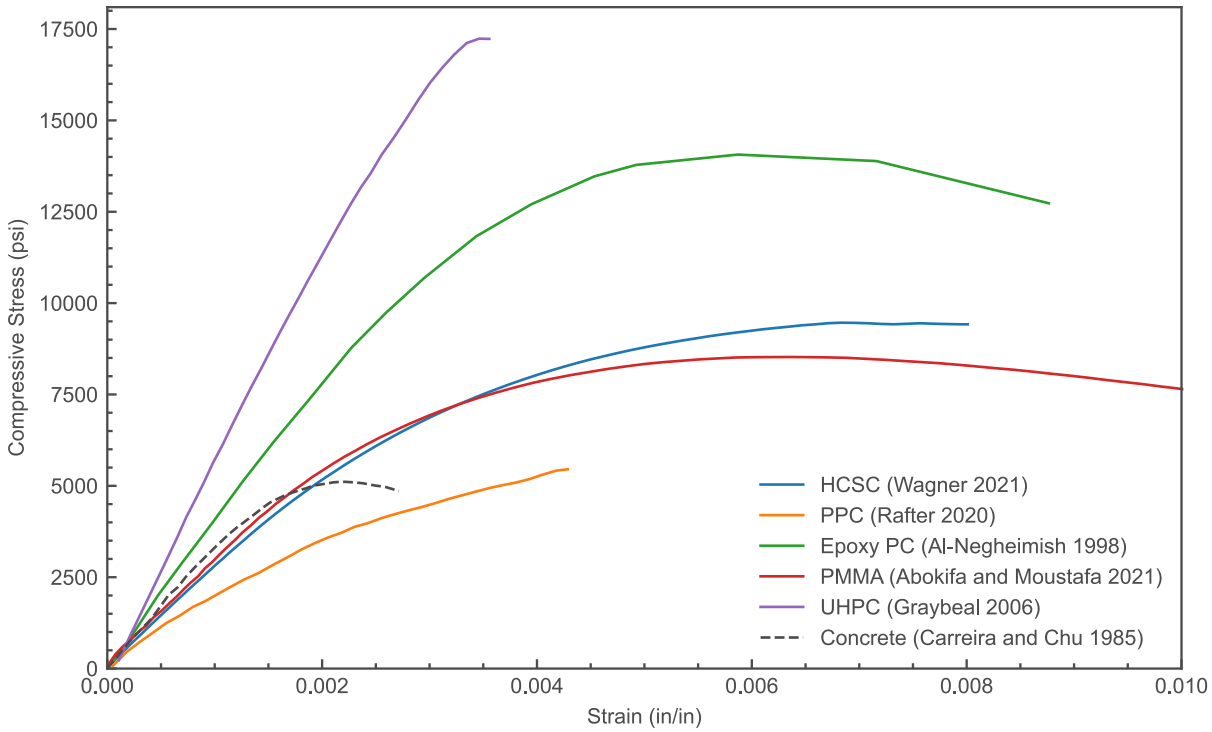

Figure 2-2. Compressive stress-strain behavior of polymer concretes at room temperature

Creep in PC depends on the creep properties of the polymer binder (ACI 2019). Hsu and Fowler (1985) found that PC has higher creep (one to two times) when compared with Portland-cement concrete, though the specific creep, the creep strain per unit stress, is approximately the same. The rate of creep is concentrated in the early stages of loading. More than 20 percent of creep at one year took place within the first day, with almost 50 percent during the first five days. Although there is more creep, the static strength of the PC members was not found to be significantly affected. When unloaded, PC exhibits both elastic and creep recovery, with the ultimate strength being minimally affected by long-term creep.

2.3.1. Temperature Effects

The influence of temperature on the properties of polymer concretes is of particular interest for ABC applications. The temperature at curing also affects the mechanical properties of PC, as the chemical reaction of cross-linking is dependent on temperature. At high temperatures, the reaction occurs too rapidly, and the elements of the reaction do not have adequate time to mix before the reaction occurs. At low temperatures, the reaction occurs too gradually, which prevents proper curing (Oussama et al. 2012).

In general, the strength of polymer concretes varies inversely with temperature. At lower temperatures, polymer concretes have higher strengths and elastic moduli and lower strain capacities when compared to the properties at room temperature. The reverse is true at higher temperatures. While this trend holds for all polymer concretes, the variation in mechanical properties as a function of temperature depends significantly on the binder chemistry. Understanding the variation in mechanical properties with temperature for commercially available polymer concretes is critical for determining design recommendations for ABC closure joint applications. Figure 2-3 shows the influence of testing temperature on the compressive strength of several polymer concretes.

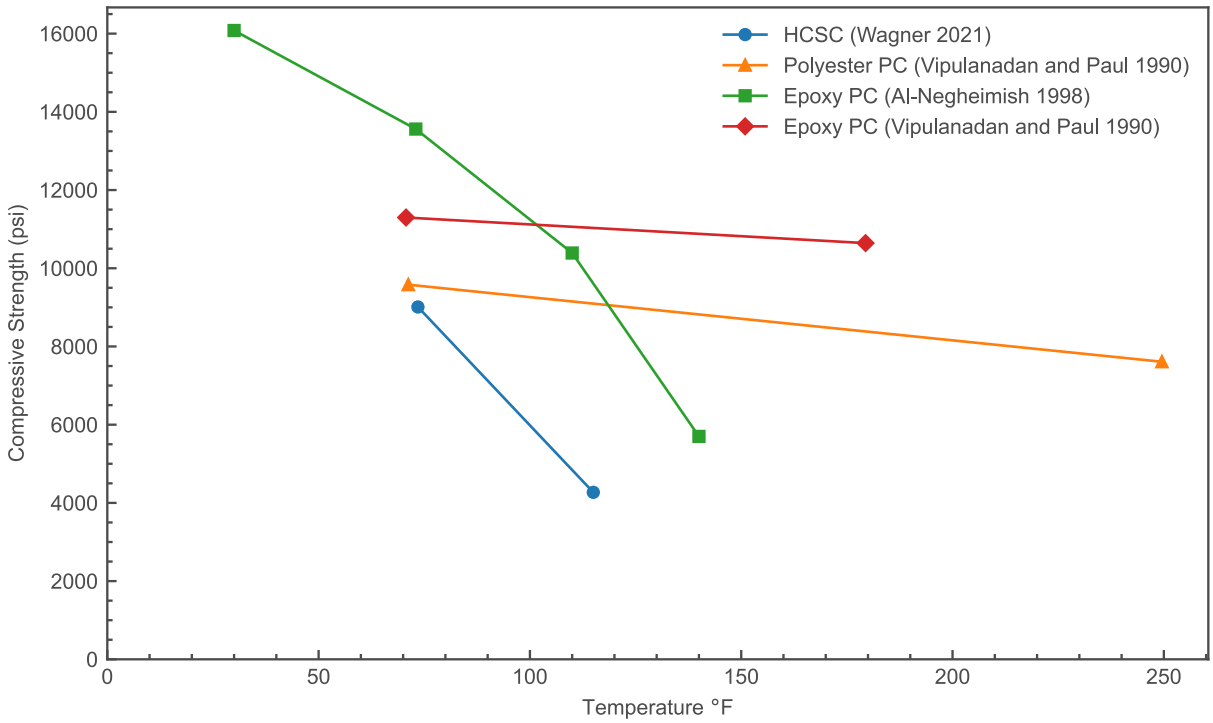

Figure 2-3. Previous studies investigating the influence of temperature on compressive strength

Researchers have investigated the influence of temperature at several different stages: during curing or hardening of the polymer binder, freeze/thaw cycling, exposure to extreme temperatures prior to testing at ambient conditions, and during the testing itself. Table 2-2 summarizes previous experimental campaigns that have considered the influence of temperature on the mechanical properties of polymer concretes.

The coefficient of thermal expansion is significant for the structural use of PCs since the PC component is rigidly attached to other materials. It is important to account for the variation of the coefficient of thermal expansion between materials to reduce cracking and ensure continuous load paths.

The coefficient of thermal expansion for PCs is typically higher than that of cementitious concretes. PCs with low resin content, around less than 10% by weight, are more influenced by

aggregate and have lower expansion coefficients. As polymer content increases, the coefficient of thermal expansion approaches that of the polymer (ACI 2019).

Shrinkage occurs in PC as the resin changes from a liquid to solid and as the specimen cools from the exothermic reaction. This is known as polymerization shrinkage. The amount of shrinkage that occurs varies based on the type of binder. Slowing curing systems and binder systems for low-shrinkage have been developed to chemically compensate for shrinkage (Maas 2003).

Table 2-2. Previous studies investigating the effect of temperature

Author	Resin/ Fibers	Temp Type	Findings
Aboutaha et al. 2005	Transpo T48A (epoxy), Flexolith (epoxy), Redeck, Strongwell, with fibers	Testing temperature	• Compressive strength and modulus of PC are higher at low temperatures and lower at high temperatures compared to room temperature. • The flexural modulus of PC increases at low temperatures and decreases at high temperatures.
Al-Negheimish 1988	Epoxy	Testing temperature	• The compressive strength of PC decreases with increases in temperature. The trend is linear between 30 °F and 110 °F with sharper decreases after 140 °F • The modulus of elasticity decreases with increases in temperature • At higher temperatures, the stress-strain curve becomes nonlinear at lower percentages of ultimate strength
Heidari-Rarani et al. 2014	Epoxy, with E-glass fibers	Freeze-thaw cycles, thermal fatigue cycles	• Freeze/thaw cycles did not change the failure mode type • Heat to cool thermal cycles increased the durability and load-bearing capacity whereas the cool to heat thermal cycles increased the risk of brittle tensile fracture • Fracture toughness was more sensitive to higher mean temperature cycles, where tensile strength was more influenced by lower mean temperature cycles
Hong 2017	Epoxy	Curing temperature	• Rapid strength gain occurs in the first 24 hours of curing, with 27% of the compressive strength after 6 hours and 70% after 24 hours for room temperatures • Higher curing temperatures increase the initial strength due to the increased rate of the reaction but has a negative effect on the final strength • Flexural strength decreased with an increase in curing temperature. Slow decreases in the strength up to 20 °C then a rapid decrease • The reinforcement bond strength exceeded the ACI recommendation of 1.7 MPa up to a curing temperature of 60 °C • Flexural strengths were highest at -10 °C and decreased with an increase in curing temperature. Specimens above 40 °C were insufficient per ACI recommendations • There is a strong correlation coefficient between compressive strength and bond and flexural strength, indicating that the bond and flexural strength can be used to draw a general conclusion from only compression strength data.

Krauss and Lawler 2018	Polyester Polymer Concrete (PPC)	Testing temperature	• For a #6 bar, bar yield or breakage occurred for embedment of 4.5 and 7.5 in ($6d_b$ or greater) at room temperature. For elevated temperatures (110 °F) the reinforcement pulled out before yielding was achieved. At an embedment of $7.5d_b$ and 3in side cover, the reinforcement had an average stress of 67700 psi at the time of pullout failure. • As embedment length increased, the bar stress at failure increased. • No significant difference in failure stress of the PC was noted for specimens with epoxy coated versus uncoated reinforcement
Oussama et al. 2012	Epoxy	Exposure temperature	• After being exposed to temperatures greater than 150 °C, the epoxy polymer displays a loss of strength, primarily due to thermo-oxidative degradation and debonding between the binder and aggregate. • After high-temperature exposure, there are significant reductions in compressive strength, up to 50% loss after exposure to 250 °C. • Increases in flexural strength were reported until 150 °C, then a reduction in strength was found. The behavior of the samples became more brittle with high-temperature exposure
Reis and Ferreira 2006	Epoxy, with glass and carbon fibers	Freeze-thaw cycles, thermal fatigue cycles	• With increases in peak temperature, the flexural elasticity decreases, and failure is more ductile, resulting in higher fracture toughness. • The high peak temperature also results in a loss of mechanical strength, due to the degradation of the cohesion between polymeric chains.
Ribeiro et al. 2003a	Epoxy, polyester, with glass and carbon fibers	Thermal expansion thermal cycle	• At higher temperatures, the coefficient of thermal expansion is higher. And at temperatures above 10 °C, the increase rate for epoxy PC is higher than polyester PC • The addition of glass fibers had no significant influence on the coefficient of thermal expansion, while carbon fibers had a strong reducing effect. • The coefficient of thermal expansion varies via a polynomial law and therefore varies continuously between -15 °C and 60 °C
Ribeiro et al. 2003b	Epoxy, polyester	Curing temperature and duration	• The curing cycle does not influence the final mechanical properties, but the time required varies with temperatures. Seven days curing at room temperature was shown to be equivalent to three hours at 80 °C.
Ribeiro et al. 2004	Epoxy, polyester	Testing temperature, conditioning temperature	• Freeze/thaw cycles between -10 °C and 10 °C resulted in little damage, potentially due to the reduced degree of water adsorption and water content • Flexural properties are highly dependent on temperature, with epoxy being more sensitive than polyester • Temporary changes in temperature have no significant influence on the flexural strength as long the specimen is returned to the original temperature.

Vipulanandan and Paul 1990	Epoxy, polyester	Curing temperature, testing temperature	• Splitting tensile strength of epoxy PC is almost unchanged but increases with curing temperature for polyester PC. • The compressive strength ratio (strength of the PC/strength of just polymer) increases with increases in temperature.
Wagner and Krauss 2020	Hybrid Composite Synthetic Concrete (HCSC)	Testing temperature	• NYSDOT pull-out tests at elevated temperatures were sufficient to develop yield stress for the tested bars and embedment length • The compressive strength of HCSC at elevated temperatures is less than the strength at room temperature.

2.4. REINFORCEMENT

Polymer concretes have tensile strengths exceeding those of conventional cementitious concrete (~1000 psi vs ~530 psi), however, reinforcement by deformed bar reinforcement or fibers is still required for structural applications.

As an additional tool for the modification of polymer concrete behavior, fibers can be added to the mixture of binder and aggregate. Fibers have been shown to increase the splitting tensile strength and ductility of the mixture and decrease the coefficient of thermal expansion, which is typically higher than that of conventional concrete and steel (ACI 2019). Possible fiber materials include steel, glass, basalt, and other recycled materials. Various studies using epoxy and polyester PC with glass, carbon, or steel fibers have been conducted and are summarized in Table 2-3. For the polymer concrete and reinforcement to work compositely, sufficient bond must exist between the two. This is a critical design parameter and is one of the major differences between cementitious and polymer concretes.

Adequate bonding between the closure joint substrate and the deformed bar reinforcing is crucial in closure joints. The development and splice length of the bar must be large enough to develop the stresses in the reinforcement. The lengths required are largely functions of the substrate material. While much is known about the required development lengths in conventional concrete, minimal research has been conducted on PCs. Mantawy et al. (2019) found that the minimal development length for steel bars embedded in Polymethyl methacrylate (PMMA) was between $3.6d_b$ to $4.1d_b$. The minimum splice length required with a concrete cover of $3d_b$ was found to be $4.1d_b$. These recommended development and splice lengths are significantly smaller than the AASHTO requirement for conventional concrete.

Abokifa and Moustafa (2021) found that PMMA adequately satisfies the AASHTO LRFD requirements of longitudinal joints. The tested deck system remained elastic without any major flexural or interface cracking in the joint. When UHPC joint geometry recommendations were used with PMMA, the results also met AASHTO LRFD standards. This indicates the field joint width for UHPC is also sufficient for PMMA in terms of load distribution.

Table 2-3. Previous studies investigating the influence of fibers

Author	Resin	Reinforcement/Fibers	Findings
Aboutaha et al. 2005	Transpo T48A (epoxy), Flexolith (epoxy), Redeck, Strongwell	Varies with proprietary blend	• Compressive strength and modulus of PC are higher at low temperatures and lower at high temperatures compared to room temperature • The flexural modulus of PC increases at low temperatures and decreases at high temperatures.
Heidari-Rarani et al. 2014	Epoxy	E-glass fibers (0.5% by weight)	• Freeze/thaw cycles did not change the failure mode type • Heat to cool thermal cycles increased the durability and load-bearing capacity whereas the cool to heat thermal cycles increased the risk of brittle tensile fracture • Fracture toughness was more sensitive to higher mean temperature cycles, where tensile strength was more influenced by lower mean temperature cycles
Reis and Ferreira 2006	Epoxy	Glass fibers (1% by weight), carbon fibers (2% by weight)	• With increases in peak temperature, the flexural elasticity decreases, and failure is more ductile, resulting in higher fracture toughness. • The high peak temperature also results in a loss of mechanical strength, due to the degradation of the cohesion between polymeric chains.
Ribeiro et al. 2003	Epoxy, polyester	Glass fibers (1% by weight), carbon fibers (2% by weight)	• At higher temperatures, the coefficient of thermal expansion is higher. And at temperatures above 10 °C, the increase rate for epoxy PC is higher than polyester PC • The addition of glass fibers had no significant influence on the coefficient of thermal expansion, while carbon fibers had a strong reducing effect. • The coefficient of thermal expansion varies via a polynomial law and therefore varies continuously between -15 °C and 60 °C
Abdel-Fattah and El-Hawary 1999	Epoxy, polyester	Uncoated rebar	• Maximum compressive strength and modulus of rupture were achieved with 12% resin content for all types of resin tested • The modulus of rupture can be up to 3 times that of Portland-cement concrete of the same ultimate compressive strength

Abokifa and Moustafa 2021	Transpo T-17 (Methyl Methacrylate)	Uncoated rebar	• PMMA reached the AASHTO ultimate load before significant cracking was observed • PMMA has a larger compressive ultimate strain, enhanced post-peak behavior, and strain deformation capacity than portland-cement concrete and UHPC • PMMA is ductile and has a sustained tensile capacity with increasing strain until cracking. Failure of PMMA in tension is brittle after the first crack is formed.
Guedes et al. 2004	Epoxy	GFRP Bar	• PC displays a linear viscoelastic mechanical behavior with the GFRP-reinforcement exhibiting linear elastic mechanical behavior for a stress level up to 45% of the ultimate load • The created model predicted a strong increase of GFRP-rebar tensile strength after 10000 hours, with the suggested consideration of creep and creep rupture of the rebar for long-term analysis
Mantawy et al. 2019	Polymethyl Methacrylate	Gr 60 uncoated rebar	• Recommended development length of 3.6-4.1 d_b in PMMA • Minimum lap splice length of $4.1d_b$ recommended with a cover of $3d_b$
Mebarkia and Vipulanandan 1992	Polyester	Glass fibers, 0-6% by weight	• An increase of fibers results in a reduction of the compressive modulus and an increase in compressive strength of 33% over unreinforced PC • Glass fibers increase the failure strain and toughness
Park et al. 2010	Polyester	Gr 60 uncoated rebar	• The actual moment of inertia of PC beams is underestimated via the ACI effective moment of inertia • The ductility indexes decrease as the ratio of tensile reinforcement increases
Reis 2005	Silicem eposil 551 (Epoxy)	Glass fibers (1% by weight), carbon fibers (2% by weight)	• The addition of fibers increases the compressive strength compared to unreinforced PC. Glass fibers resulted in an increase of 27.5-45.4% and 36.1-55.1% for carbon fibers. • Fibers also result in a slightly more ductile failure; unreinforced PC displays a brittle failure

Sett and Vipulanandan 2004	Polyester	Glass fibers, carbon fibers, 0-6% by weight	• The optimum polymer content is 14% when unreinforced. With 6% glass fibers, 18% polymer is optimal for strength and workability. For 6% carbon fibers, 20% polymer is optimal for workability and tensile strength. • Tensile strength of PC is improved by 85% and 60% from the addition of 6% fibers, glass, and carbon respectively. • Glass fibers improved the compressive strength of PC, but carbon fibers did not have a significant difference • Both types of fibers increased the damping ratio for longitudinal modes
Vipulanandan and Mebarkia 1996	Polyester	Glass fibers, 0-6% by weight	• The addition of 6% glass fibers with 18% polymer content resulted in an 80% increase in flexural strength compared to unreinforced PC. • Silane-treated aggregates and fibers doubled the flexural strength for a mix including 6% glass fibers and 18% polymer content. • Based on the stress intensity factor, crack resistance curved can be linearly approximated

CHAPTER 3. MATERIAL CHARACTERIZATION

The complete testing program was broken down into two phases – the first of which was to characterize the mechanical properties of a commercially available FRPC material (compressive strength, flexural strength, and tension strength) at several test temperatures and ages using standard test methods that would be part of a typical quality control program.

3.1. COMMERCIAL PRODUCTS

The use of commercially available products was preferred so that the results of the research were scalable. A commercially available FRPC material was identified, Kwik Bond Polymers' Hybrid Composite Synthetic Concrete (HCSC). HCSC comprises a urethane vinyl ester hybrid copolymer resin binder, graded silica aggregates, and pre-blended basalt chopped fibers. The initiator used is MEKP and the accelerator is a propriety blend called Z-cure. An HMWM primer was used in conjunction with the binder for bonding HCSC to concrete and steel substrates. Table 3-1 compares the manufacturer provided mechanical properties of HCSC to UHPC and other commercially available polymer concretes.

Table 3-1. Summary of PPC and HCSC Mechanical Properties

Material (Manufacturer)	**UHPC**	**MMA (Transpo)**	**PPC (Kwik Bond)**	**HCSC (Kwik Bond)**
Compressive Strength	24000 psi	9000 psi	6000 psi	10000 psi
Tensile Strength	1200 psi	1200 psi	800 psi	1500 psi
Modulus of Elasticity	7000 ksi	1200 ksi	1500 ksi	2500 ksi
Coefficient of Thermal Expansion	6-8 x 10^{-6} in/in/°F	-	<10 x 10^{-6} in/in/°F	<11 x 10^{-6} in/in/°F
Development Length	~8 d_b	~4+* d_b	~6* - 10** d_b	~6** d_b

* At room temperature
** At elevated temperature

3.2. MATERIAL COMPONENTS

Table 3-2 summarizes the mixture design recommended by the manufacturer and used in this study. Each test series was poured with one mixed batch of approximately 230 lbs of prebagged aggregate and basalt fiber mix. Particular ratios of the components can be adjusted, as appropriate, to increase workability and accelerate curing.

Table 3-2. HCSC mix design

% Binder (by mass Aggregate)	% MEKP (by mass Binder)	% Z-cure (by volume MEKP)
13.5%	2.20%	3.00%*

*Z-cure volume as specified by Kwik Bond representative

For tests that included a cold joint or deformed bar reinforcement, HMWM primer was applied to the bond surface before casting HCSC per the manufacturer's recommendation. The HMWM primer is mixed with Z-cure as the accelerator and cumene hydro peroxide (CHP) as the initiator. Table 3-3 shows the mixture proportions specified by the manufacturer.

Table 3-3. HMWM primer mix design, by volume

Pro-Prime (HMWM)	CHP	Z-cure
128 parts	3 parts	1 part

Accelerator

Table 3-4 shows the working time and time to 70% of the 7-day compressive strength, for three levels of the accelerator, measured as a volume ratio to the initiator. The volume of the accelerator can be adjusted to achieve a range of working and curing times or to accommodate specific site conditions (cold/hot weather). At the start of the project, several trial batches were performed to determine the appropriate level of the accelerator to use for the remainder of the test series. The

table clearly shows the tradeoff between working time and the time required to achieve strength. If shorter working times can be tolerated, significant strength (70% of the 7-day value) can be achieved 2 hours after mixing. In the laboratory, a value of 3% accelerator by volume initiator was selected as a compromise between working time and time required for predetermine strength gain.

Table 3-4. Normalized compressive strength and working time for various accelerator volumes

Accelerator by volume initiator	Approximate working time	Time to 70% of 7-day compressive strength
1%	20 min	4 hrs
3%	16 min	4 hrs
8.3%	7 min	2 hrs

3.3. MIXING PROCEDURE

Figure 3-1 shows the mixing procedure for the particular equipment used in this study. Each test batch was mixed in the laboratory using a standard drum mixer; however, in a field application, mixing would typically be completed using a volumetric mix truck to accommodate the required quantity of materials. Each batch was approximately 1.9 CF. The mixing procedure is comprised of four major steps:

1. If needed, mix HMWM per the manufacturer's recommended proportions and apply HMWM primer to the bond line and reinforcement. HCSC should be placed between 15-120 minutes after priming.
2. Mix HCSC resin with MEKP and Z-cure accelerator using a standard squirrel cage mixer until incorporation, around 45 seconds.
3. Add approximately 2/3rds of the resin mixture to the drum mixer then add approximately 2/3rds of the pre-package aggregate and fiber blend. Mix in the drum mixer until loosely incorporated.

4. Add in the remaining aggregate and fiber mix and the remainder of the resin blend. Mix for roughly two minutes.

Figure 3-1. (a) Mixing of MEKP and HCSC resin with a squirrel cage mixer, (b) Resin mixture being transferred from mixing bucket to drum mixing, (c) Adding the pre-packaged aggregate and fiber blend to the drum mixer, (d) HCSC mix turning in drum mixer, (e) HCSC placed in cylinder molds before finishing

3.4. SPECIMEN FABRICATION

Before mixing the HCSC, all formwork was prepared to help demold the HCSC after curing. Plastic molds were used for all cylinders, beams, and pullout specimens. Beam molds were sprayed

with a release agent. Medium-density overlay (MDO) was used as formwork for cementitious concrete casting, and melamine was used for HCSC casting in non-contact splice specimens.

Once mixed, the following procedure was followed for all HCSC specimens:

1. Discharge HCSC
2. Fill specimens until half-full. Vibrate cylinders, beams, and bond pullout specimens on a vibrating table for approximately 30 seconds until well consolidated. For non-contact splice specimens consolidate with hand vibration and rod corners.
3. Fill specimens until full. Vibrate for another 30 seconds.
4. Hand finish with a trowel.
5. For temperature conditioned specimen, cure for 24 hours at ambient temperatures uncovered. For strength gain over time specimen, cure at ambient temperatures uncovered until testing time
6. Demold specimens. For temperature conditioned specimen, wait until 7-days post HCSC pour to begin conditioning or testing.

3.5. TESTING SETUP

Figure 3-2 shows the experimental setups and HCSC test specimens for the material characterization testing. The development of mechanical properties over time and the influence of temperature on the mechanical properties of cured HCSC were investigated by experimentally testing beam, cylinder, and bond specimens under monotonic loads to failure.

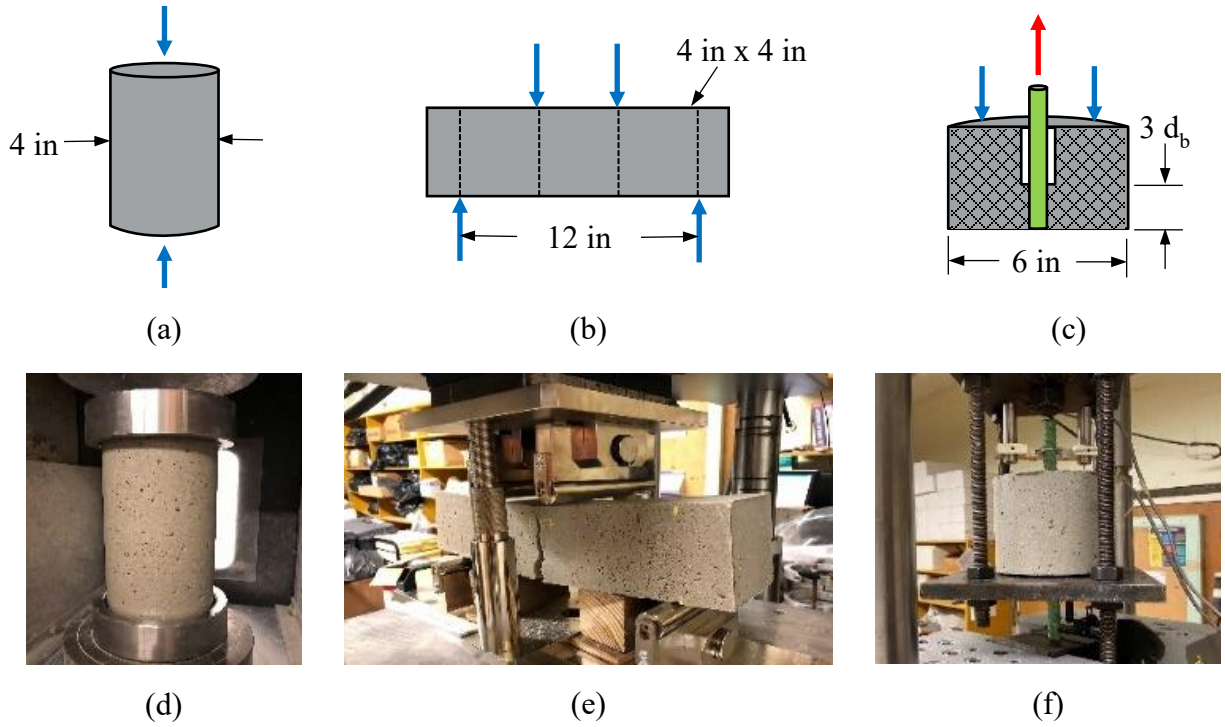

Figure 3-2. Diagrams and test setup for (a/d) compressive strength, (b/e) modulus of rupture, (c/f) bond pullout

Compressive strength tests were conducted according to ASTM C39 (ASTM 2021a). Flexural strength tests were conducted according to ASTM C78 (ASTM 2021b). Pullout bond cylinders were tested following the procedures of ASTM D7913 (ASTM 2020a), however, the specimen size was reduced and epoxy-coated reinforcement was used. Given the higher tensile strength of HCSC in comparison to conventional concrete that is used in the ASTM D7913 standard, this reduction was deemed appropriate. This provided a measure of the pure bond strength when failure occurred by reinforcement pullout, which was later used in determining the experimental design parameters for non-contact splice testing. The testing procedure used was similar to that of Peruchini et al. (2017) who tested bond pullout cylinders with UHPC.

Figure 3-3a shows the pullout bond cylinder specimens under construction. An epoxy-coated #5 rebar was cast in the center of a 6 in diameter by 6 in tall cylinder mold. The bottom four inches

of the rebar were debonded from the HCSC by placing a PVC tube around the rebar and sealing the top and bottom. This resulted in a two-inch bonded length and ensured a pullout failure mode instead of splitting of the polymer concrete. Figure 3-3b and Figure 3-3c show the test configuration. The specimens were suspended by the bottom face (closest to the debonded section) via a steel plate with a hole in the middle, and the bottom portion of the rebar was gripped by the testing machine. Two LVDTs, oriented at 180 degrees from each other, were placed four inches above the hand-finished top face of the specimen to record the pullout of the reinforcement relative to the top (back) face of the cylinder.

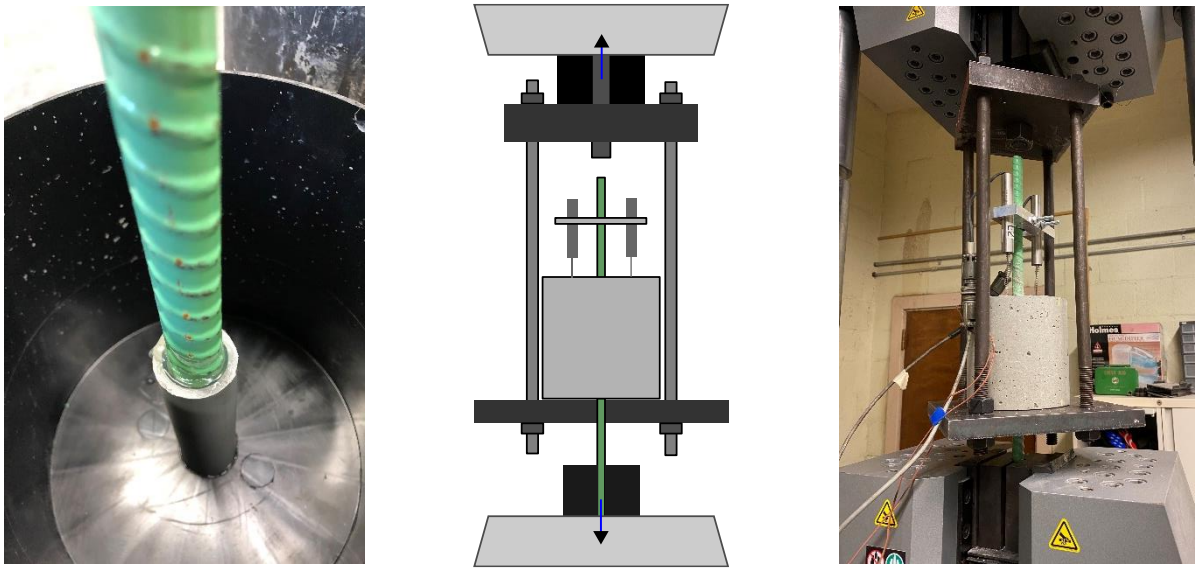

(a) (b) (c)

Figure 3-3. (a) Debonded section of the specimen, (b) test diagram, (c) testing setup

For each strength test, two batches of HCSC specimens were cast. One batch of specimens was tested at various temperatures and one batch was tested at various times throughout the curing process. Table 3-5 shows the approximate intervals and number of specimens tested for each strength test. For each batch of specimens, the 7-day compressive strength of the HCSC was also determined and used as a control test to ensure consistent batching, mixing, and curing of the HCSC throughout the testing program.

Table 3-5. Mechanical property specimen catalog

Test Type	Parameter	Approximate Interval	Number of Specimens
Compression	Time-Strength (hrs)	2, 2.5, 3, 3.5, 4, 5, 6, 7, 8	1 per time plus 3 at 7 days, 12 total
	Temperature (°F)	10, 45, 80, 115	3 per temperature, 12 total
Flexure	Time-Strength (hrs)	2, 3, 4 ,5 ,6 ,8 ,12, 24, 72	1 per time plus 3 at 7 days, 12 total
	Temperature (°F)	10, 45, 80, 115	3 per temperature, 12 total
Bond Pull	Time-Strength (hrs)	2, 2.5, 3, 4, 6, 8, 12, 24, 72	1 per time plus 3 at 7 days, 12 total
	Temperature (°F)	10, 45, 80, 115	3 per temperature, 12 total

3.6. COMPRESSIVE STRENGTH OF 7-DAY CONTROL CYLINDERS

The reserved cylinders from each batch were tested at 7-days and ambient temperatures. Figure 3-4 shows the distribution of compressive strength. The results show that the compressive strength of the cast HCSC was roughly 9200 psi and was consistent between the 24 cylinders, indicating low batch-to-batch variability of compressive strength.

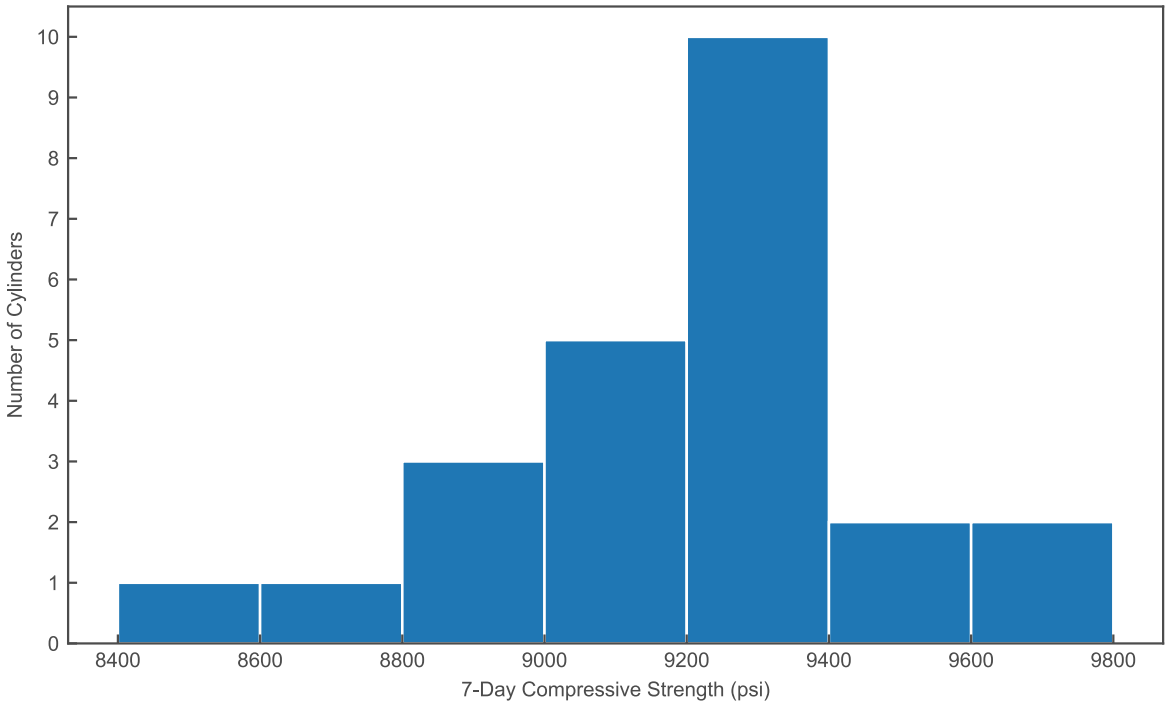

Figure 3-4. Histogram of 7-day compressive cylinder strengths

3.7. TEMPERATURE RISE DURING HARDENING

Polymer concretes are typically made using thermosetting resins and, therefore, cure exothermically. Thermocouples were embedded in at least one specimen per batch to determine the temperature of specimens during conditioning and testing. Thermocouples were placed in the specimens such that they were in the center of the cross-section and would not disrupt the loading or impact the failure method. Figure 3-5 shows the exothermic behavior of cross-linking in HCSC during the curing process. The peak temperature for the material characterization is roughly 120 °F. The temperature variation can be attributed to the variation in specimen size, and thus overall thermal mass, mold type and thickness, and ambient temperature.

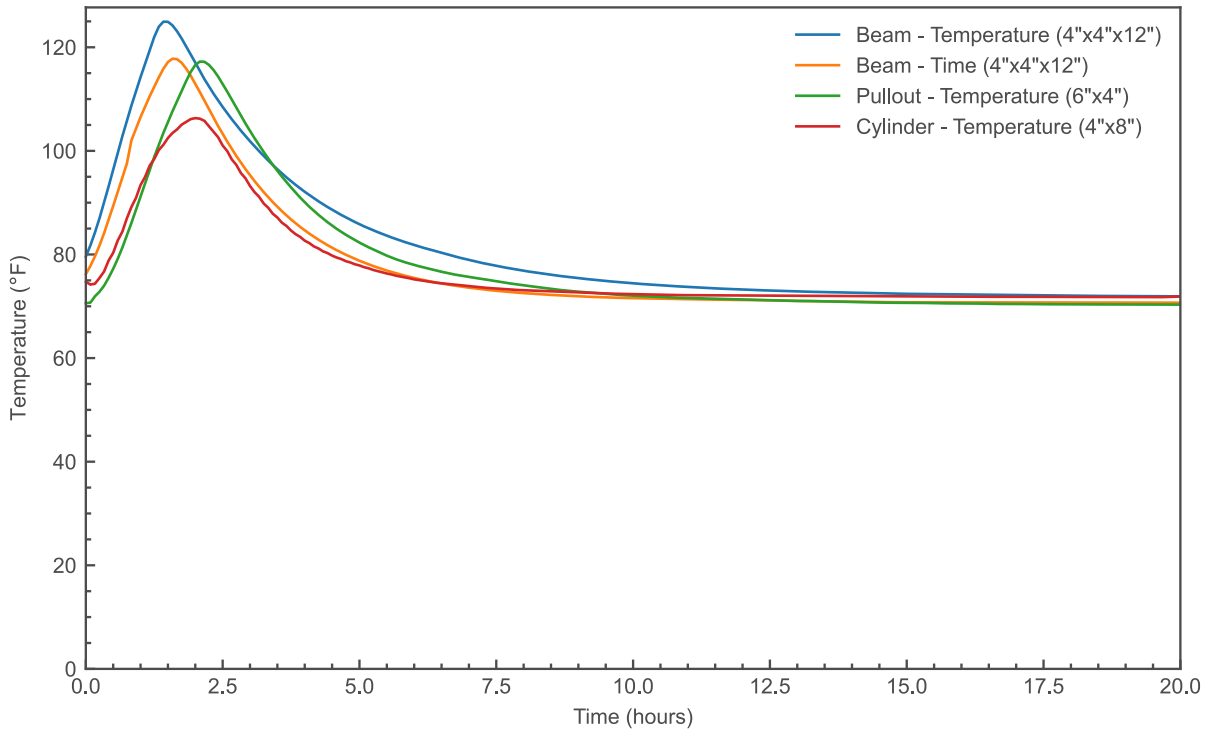

Figure 3-5. Temperature of specimens during curing

3.8. STRENGTH GAIN OVER TIME

To quantify the evolution of mechanical properties over time, especially the strength gain over the first few hours after mixing, test specimens (cylinders, beams, bar pulls) were cast and allowed to cure under ambient conditions (roughly 75 °F and 45% RH). Starting at the earliest feasible time (determined to be 2 hours after mixing), specimens were removed from their molds and tested to failure at least every hour, until 8 hours after mixing. The remaining specimens were tested at convenient intervals, and three specimens were reserved for testing at 7 days.

Figure 3-6 shows the force-displacement response curves and static modulus of elasticity for beams as a function of time after mixing.

Table 3-6 summarizes the beam stiffness and modulus of elasticity at each testing time. The response was fit with a linear curve, as the initial part of the response is non-linear due to excess slack in the testing system. The line was then projected backward to zero, to allow for a comparison

of the material stiffness at different curing times. The beam tested 2 hours after mixing has a slight non-linear response before failure. For specimens tested later, the behavior becomes more linear and is stiffer. The beams that were tested at 7 days after mixing, and those tested at room temperature between both batches have a similar stiffness, indicating consistency in the specimens between batches. Based on the slope of the linear portion of the response, the dimensions of the beam, and the loading geometry, the static modulus of elasticity was also calculated. Similar to the stiffness of the beams, there is a rapid increase in the modulus of elasticity, the rate of this increase then tapers off after approximately 8 hours.

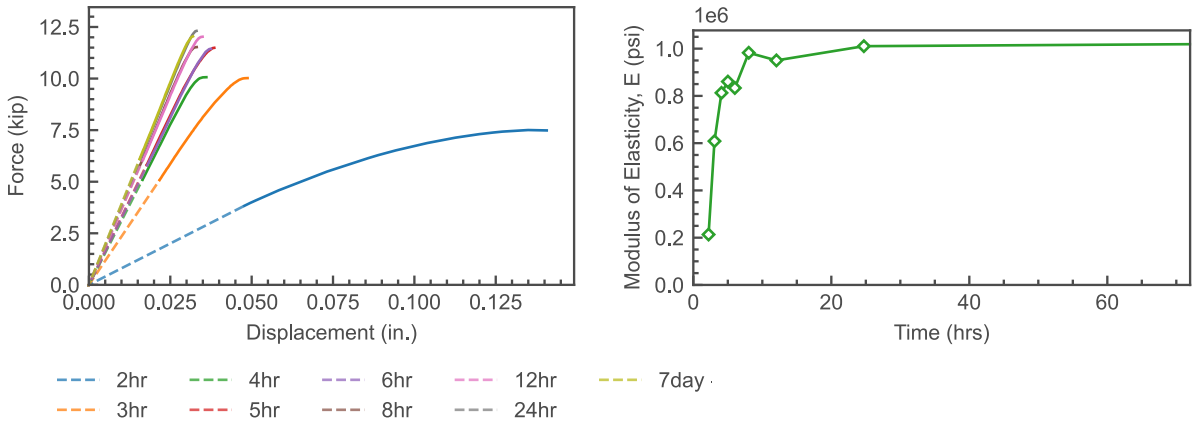

Figure 3-6. Beam stiffness and modulus of elasticity as a function of time after mixing

Table 3-6. Beam stiffness and modulus of elasticity as a function of time after mixing

Time (hrs)	Stiffness (kip/in)	Modulus of Elasticity (psi)
2	80.2	2.13×10^5
3	234.3	6.09×10^5
4	310.3	8.13×10^5
5	328.5	8.61×10^5
6	323.9	8.34×10^5
8	369.6	9.83×10^5
12	366.2	9.50×10^5
24	387.4	1.01×10^6
168 (7 days)	391.8	1.04×10^6

Figure 3-7 shows the bar stress with respect to the back end slip of the reinforcement. The behavior of the stress-slip curves shows that as the load and bar stress initially increase, there is minimal slip. Once the maximum bar and bond stress is reached, all curves soften with reduced bar stress and increasing amounts of slip. For all tests except the 7-day test, yield stress of the reinforcing was not reached, therefore measured elongation due to bar yielding is minimal. The measured slip is therefore a result of the movement of the reinforcement through the polymer concrete as the lugs of the reinforcement slip and are pulled through despite mechanical interlocking. As the stress-slip begins curve begins to flatten, resistance to slip is mostly due to residual bond stress resulting from the friction between the reinforcement and the concrete. As the material continues to cure and strengthen, the maximum bar stress increases with decreasing amounts of slip before peak bar stress.

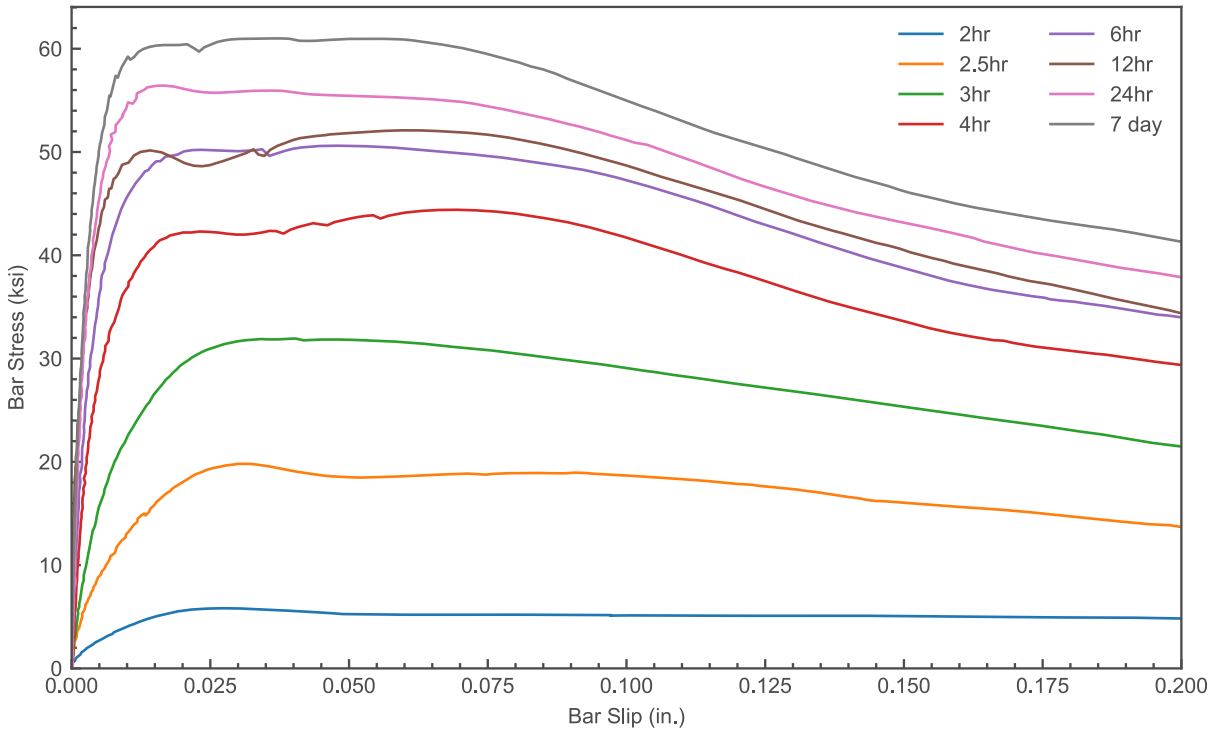

Figure 3-7. Stress-back end slip for bond pullout testing as a function of time after mixing

Figure 3-8 shows the development of the three testing strengths as well as the normalized strength as a function of time after mixing. The normalized strengths were calculated by dividing the compressive or flexural strength data by the corresponding 7-day values (i.e., the normalized strength at 7 days is exactly 1.0). Several observations can be made:

- All three curves asymptotically approached the 7-day value, as expected.
- The development of flexural strength occurred sooner than the development of the compressive strength or bond, although the three curves are very similar. This is consistent with observations made by others for cementitious concretes (e.g., Peruchini et al. 2017) although the behavior is seen here on a scale of hours rather than days.
- By 4 hours after mixing, the compressive, flexural, and bond strengths were 70%, 80%, and 75% of their 7-day values, respectively. This would likely be sufficient to allow opening of the bridge being built or reopening of a repair to traffic.
- The development of strength occurs shortly after peak curing temperatures. This could be implemented in the field as a rough indicator of strength.

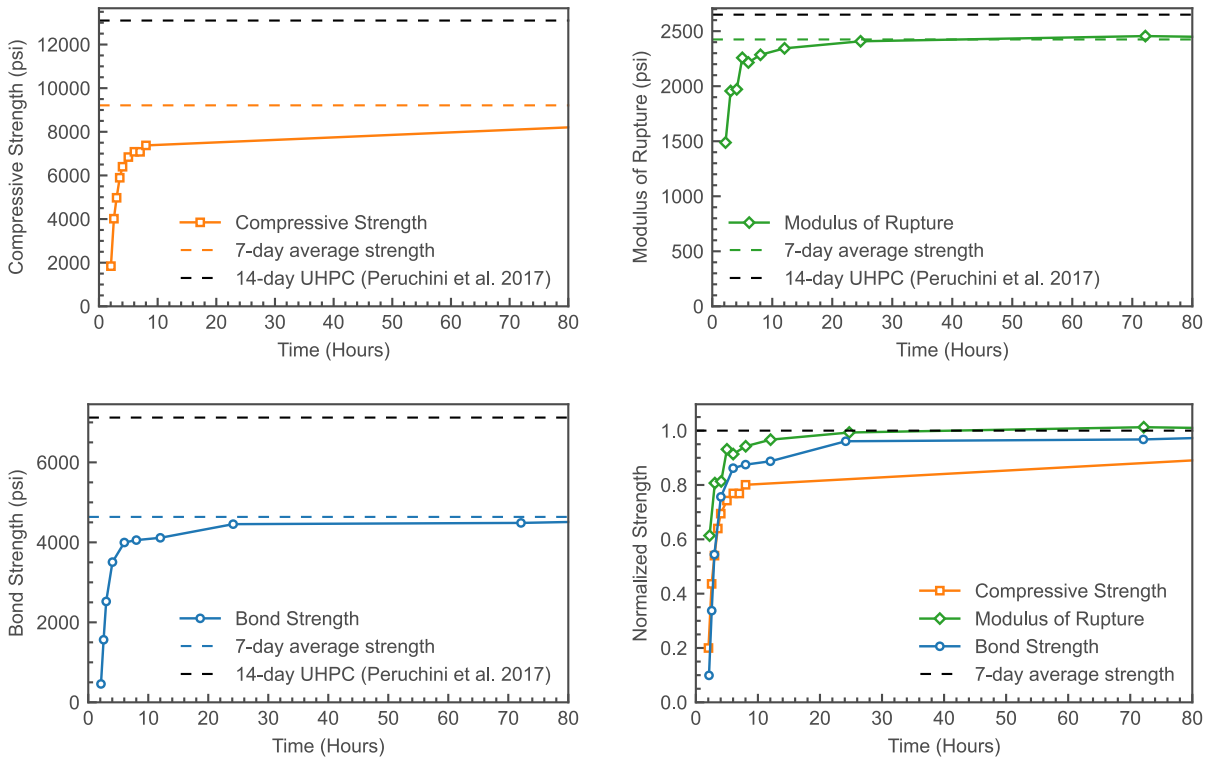

Figure 3-8. Strength (compression, flexure, bond, normalized) as a function time after mixing

3.9. INFLUENCE OF TESTING TEMPERATURE

To elucidate the influence of temperature on the mechanical properties of HCSC, test specimens (cylinders, beams, bar pulls) were cast and allowed to cure under ambient conditions (roughly 75 °F and 45% RH) for 7 days. The specimens were then conditioned to the target test temperatures (10 °F, 45 °F, 115 °F) using temperature-controlled cabinets. The specimens were kept in the temperature-controlled cabinets for at least 16 hours prior to testing to achieve the desired internal temperature, monitored by embedded thermocouples in select specimens. The specimens were then removed, one by one, from the cabinets and tested promptly. The surface temperature of the specimens was recorded before and after each test. Three specimens per temperature were tested. A set of specimens were also tested under ambient conditions at 7 days for reference.

Figure 3-9 shows the force-displacement response curves and static modulus of elasticity for beams as a function of testing temperature. Table 3-7 summarizes the average stiffness and modulus of elasticity for each testing temperature. The response was fit following the same procedure as the beams in Figure 3-6. Beams tested at higher temperatures have a shallower slope, indicating less stiff behavior. As the testing temperature decreases, the stiffness and modulus of elasticity increases.

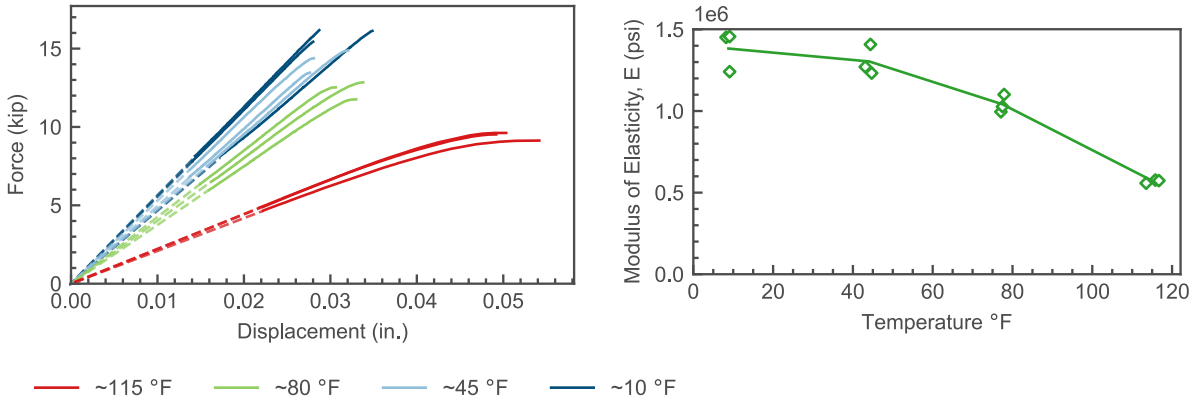

Figure 3-9. Beam stiffness and modulus of elasticity as a function of test temperature

Table 3-7. Beam stiffness and modulus of elasticity as a function of test temperature

Average Temperature (°F)	Stiffness (kip/in)	Modulus of Elasticity (psi)
8.8	528.6	1.38×10^6
44.1	500.4	1.30×10^6
77.5	400.7	1.04×10^6
115.3	217.4	5.69×10^5

Figure 3-10 shows the bar stress with respect to the back end slip of the reinforcement. The general stress-slip behavior is similar to Figure 3-7. For lower temperatures, there is less slip during the initial phase of loading before maximum bar stress than compared to warmer temperatures. For specimens tested at room temperature and colder, bar yield was reached. As the testing temperature decreases a plateau appears around the peak bar stress as the back end slip increases with little

change in the bar stress. This behavior is similar to that of well-confined concrete. This can be attributed to the high material strengths and resistance to splitting at lower testing temperatures.

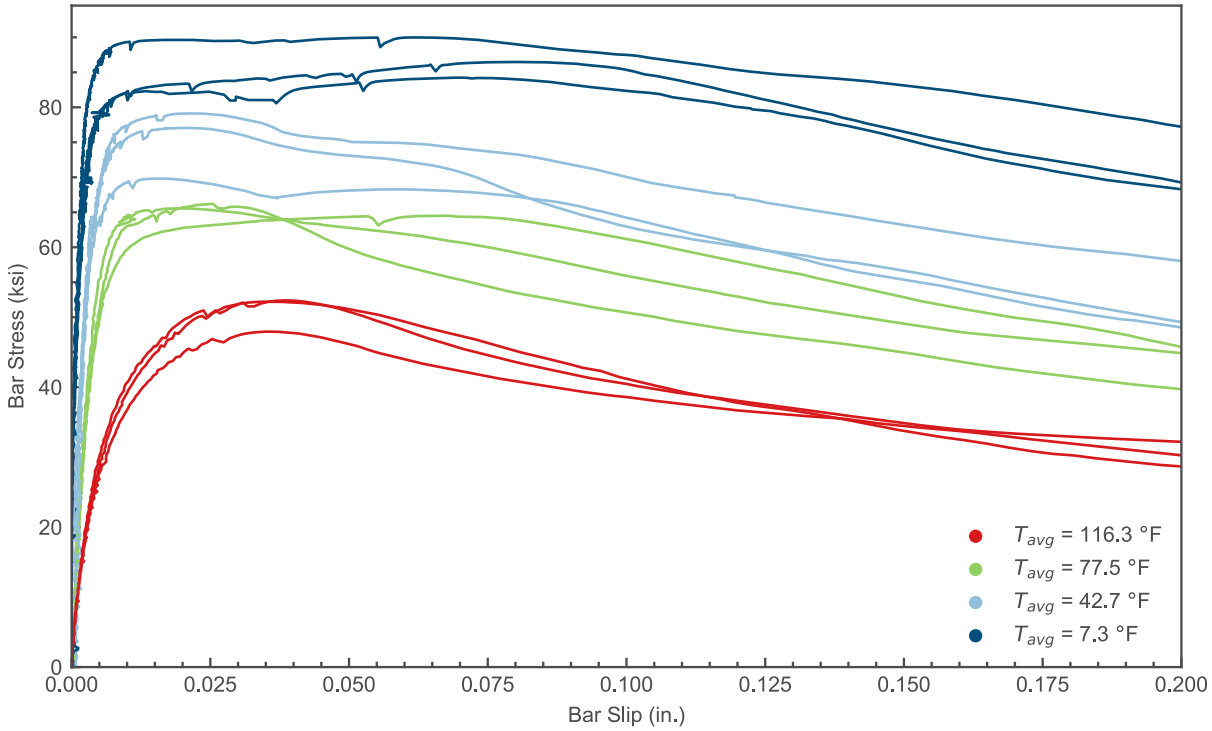

Figure 3-10. Stress-back end slip for bond pullout testing as a function of testing temperature

Figure 3-11 shows the influence of testing temperature on the mechanical properties of the test samples. The normalized strength was calculated by dividing the strength data by the corresponding average ambient temperature value, was used here to enable comparison between the three strengths (compression, flexure, and bond), and was plotted against the surface temperature at the time of testing. Deviation from the target temperature was evident in the data, due to changes in specimen temperature during handling and setup. Several observations can be made:

- The variation in mechanical properties with temperature was consistent between the three sets of tests.

- The material strengths were higher at cooler temperatures and lower at elevated temperatures when compared to strengths measured at room temperature.
- The relationship between strength and temperature was roughly linear.
- A temperature change of 40 °F resulted in a roughly 25% change in material strength, a significant variation that must be accounted for in design. For a unit change of 1 °F, there is a change of 0.6% of the normalized strength

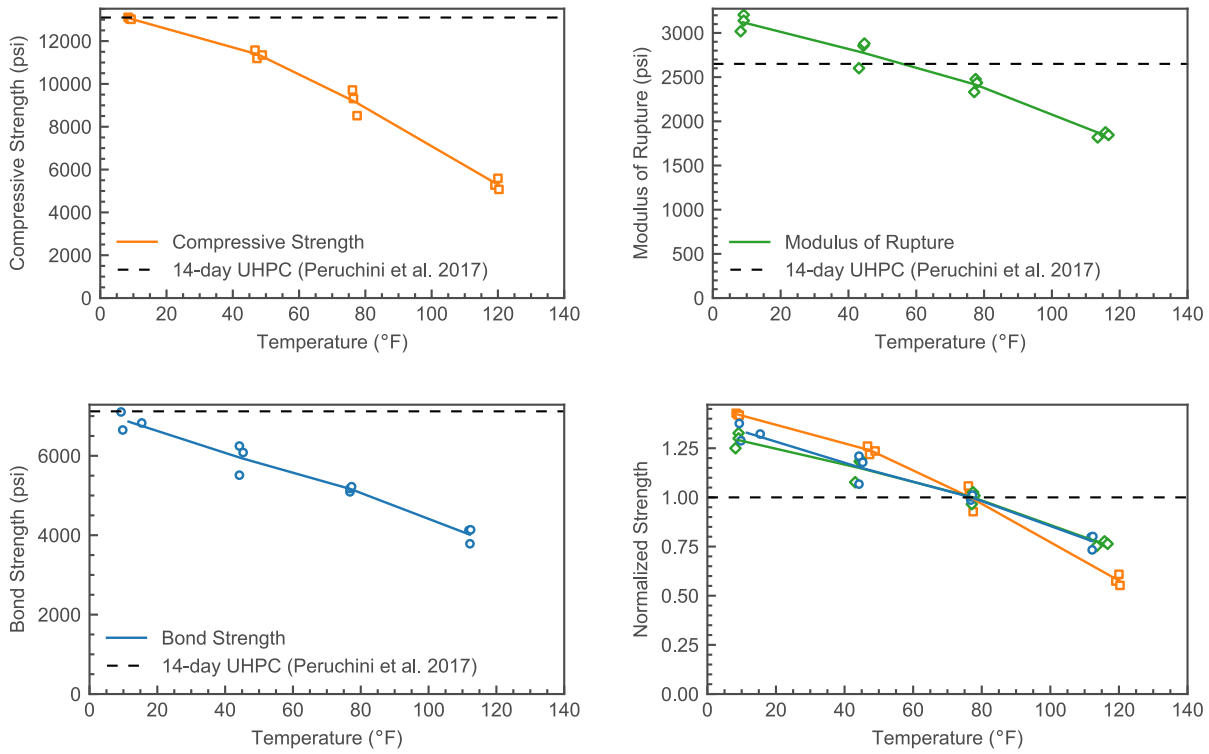

Figure 3-11. Strength (compression, flexure, bond, normalized) as a function of test temperature

The linear nature of the change in strength due to temperature was further investigated by fitting each test along with the normalized values to a regression line, Figure 3-12.

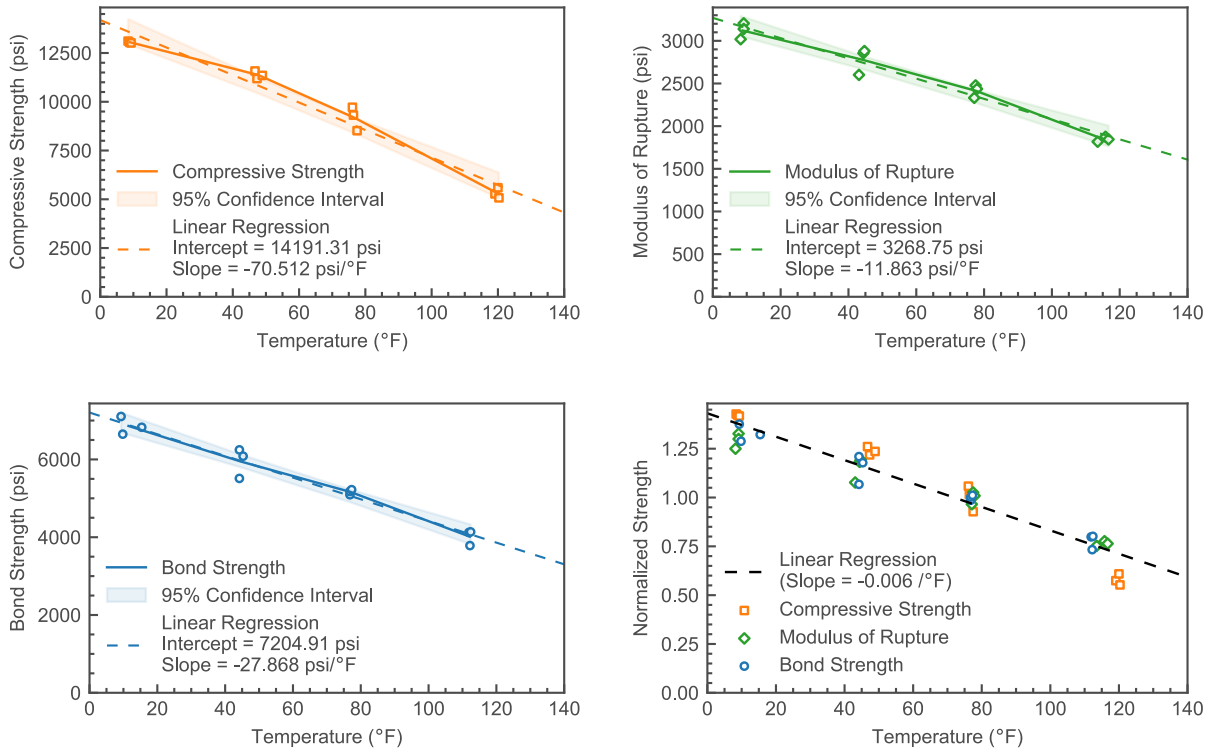

Figure 3-12. Linear Strength Regression (compression, flexure, bond, normalized) as a function of test temperature

CHAPTER 4. NON-CONTACT SPLICE TESTING PROGRAM

4.1. DESIGN OF EXPERIMENTS

To characterize the effects of various parameters on bond, non-contact splice tests were performed on epoxy-coated deformed bars embedded in FRPC. The tests focused on a simplified, non-contact splice configuration that isolates the behavior of reinforcement in a closure joint. The test setup and parameters are similar to previous studies by Qiao et al. (2016) for testing non-contact splices embedded in UHPC. Yuan and Graybeal (2014) also conducted pullout tests to evaluate the factors that affect bond strength between deformed reinforcing and UHPC. The pullout tests performed by Yuan and Graybeal were the first to investigate UHPC as a closure joint material. Many other studies following the initial research have also used a version of this setup. The test setup used by Yuan and Graybeal is shown below, Figure 4-1.

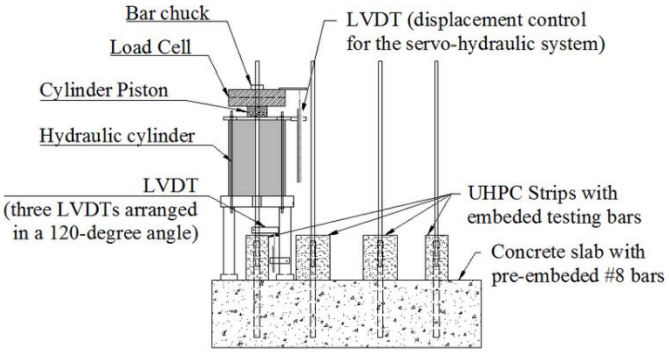

Figure 4-1. Loading setup by Yuan and Graybeal (2014)

Figure 4-2a shows the specimen geometry that was used in this project. Specimens were sized such that they could be conditioned to different test temperatures using conventional laboratory equipment and tested using a universal testing machine under precise displacement control.

Figure 4-2b shows the test configuration that was used for the tests, which was similar to the configuration used by Yuan and Graybeal (2014). The use of a full-width precast slab, similar to

Figure 4-1, would have increased the test complexity and cost and has not been shown to significantly influence the performance of non-contact splice specimens in previous studies (Graybeal and Yuan 2014, Haber and Graybeal 2018); neither concrete damage in the precast slabs nor tension failure between the UHPC strip and the precast concrete were reported during either of these test series. Instead, steel fixtures were used to anchor the reinforcement instead of a slab. A precast concrete "strip" between anchor bars, roughly equal in size to the FRPC strip and below the splice was used to stiffen the specimen. An exposed aggregate roughened surface was provided on the precast concrete strip, the surface was primed using HMWM, and HCSC was cast against it in the horizontal position, mimicking the field orientation of the joint.

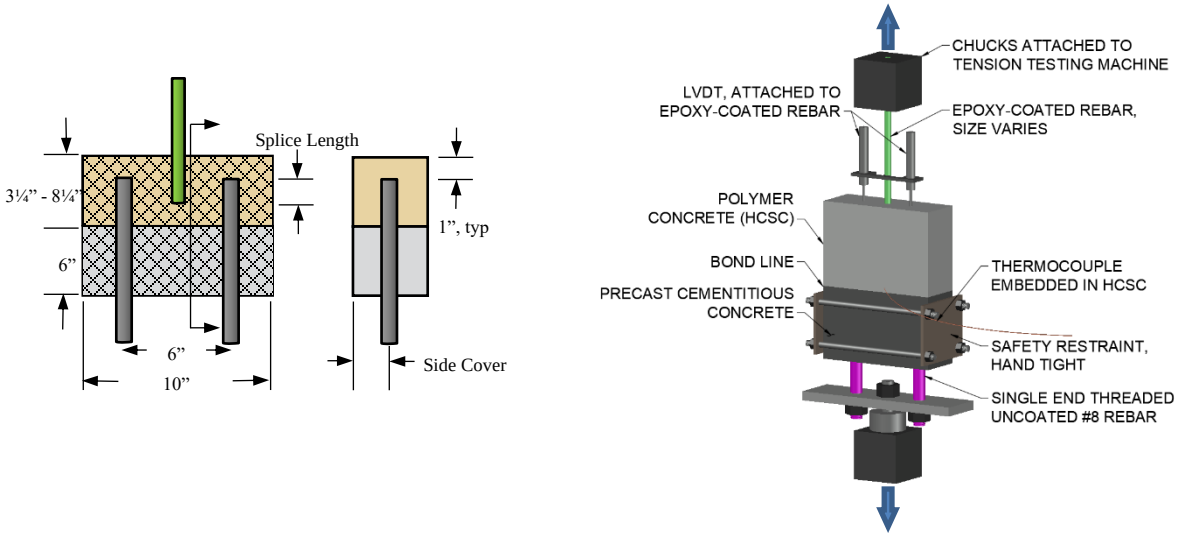

(a) (b)

Figure 4-2. (a) Elevation and section view of non-contact splice specimen, (b) diagram of testing setup

Table 4-1 and Table 4-2 show the non-contact splice test plan. The experimental matrix for this test series was constructed as a rotatable central composite design (CCD) (Box et al. 2005), with the varied parameters being test temperature, T; splice length, ℓ_s; side cover, c_b; and bar diameter, d_b. The CCD design included an embedded factorial design, repeated center points to quantify batch-to-batch uncertainty, and additional axial points that allowed for the estimation of curvature

in the region of interest. The experimental design was centered around the point (T =75 °F, ℓ_s = 3.75 in, c_b = 2.0 in, and d_b = 0.625 in) in the parameter space. Factorial or cube points are parameter levels that are a specified amount, n, above and below the center point. As part of the CCD design, multiple parameters are changed between specimens. Axial points are the extreme points where only one parameter is modified with respect to the center point. Axial points are located 2n above and below the center point. The tests were conducted in three sets, or "blocks", comprising 10 specimens apiece. Each block of specimens was made from the same batch of HCSC. The specified run number was used as an identifier for each specimen and also indicates that a full design was used with all axial and factorial combinations specified by a standard CCD design.

Table 4-1. Summary of test parameters

Bar size	Temperature (°F)	Side Cover (in.)	Overlap length (in)
No. 3	5 °F	0.75	1.25
No. 4	40 °F*	1.375*	2.5*
No. 5*	75 °F*	2*	3.75*
No. 6	110 °F*	2.625*	5*
No. 7	145 °F	3.25	6.25

*Parameters used in scoping study (Batch 0)

The parameters chosen for non-contact splice testing encompass typical values for closure pours in western Washington and many other parts of the United States.

- Bar size was centered around No. 5 bars, typical for the deck reinforcement of prefabricated superstructure components. In all tests, bar spacing of the uncoated bars was held constant at 6 in, center-to-center.
- Test temperatures encompass summer highs and winter lows in western Washington centered around a temperature that is slightly above standard room temperature (75 °F). Tests were completed at ambient lab temperatures.

- Bar cover, expressed here as the distance from the edge of the specimen to the center of the reinforcement, is consistent with tests performed by Peruchini et al. (2017), Qiao et al. (2016), and Yuan and Graybeal (2014).
- The overlap length or splice length is based on the calculated embedded lengths for reinforcement yield and fracture from the mechanical characterization findings. Based on the data, the embedded length required to yield a No. 5 epoxy-coated bar varied from 1.5 in. to 2.6 in. for the range of temperatures tested. The embedded length needed to fracture a No. 5 bar varied from 2.2 in. to 3.8 in. The overlap length used here is necessarily longer, accounting for differing test configurations, the spacing between bars in the non-contact splice, and the reduction in side cover.

Table 4-2. Non-contact splice experimental matrix

	Run	Temperature T (°F)	Splice length ℓ_s (in)	Side Cover c_b (in)	Bar diameter d_b (in)	Point Description
Block / Batch 1	1-01	40	5	1.375	0.5	Factorial
	1-02	40	2.5	2.625	0.5	Factorial
	1-03	110	2.5	1.375	0.5	Factorial
	1-04	110	5	2.625	0.5	Factorial
	1-05	40	2.5	1.375	0.75	Factorial
	1-06	40	5	2.625	0.75	Factorial
	1-07	110	5	1.375	0.75	Factorial
	1-08	110	2.5	2.625	0.75	Factorial
	1-09	75	3.75	2	0.625	Center
	1-10	75	3.75	2	0.625	Center
Block / Batch 2	2-01	40	2.5	1.375	0.5	Factorial
	2-02	40	5	2.625	0.5	Factorial
	2-03	110	5	1.375	0.5	Factorial
	2-04	110	2.5	2.625	0.5	Factorial
	2-05	40	5	1.375	0.75	Factorial
	2-06	40	2.5	2.625	0.75	Factorial
	2-07	110	2.5	1.375	0.75	Factorial
	2-08	110	5	2.625	0.75	Factorial
	2-09	75	3.75	2	0.625	Center
	2-10	75	3.75	2	0.625	Center
Block / Batch 3	3-01	75	3.75	2	***0.375***	Axial
	3-02	75	3.75	2	***0.875***	Axial
	3-03	***5***	3.75	2	0.625	Axial
	3-04	***145***	3.75	2	0.625	Axial
	3-05	75	3.75	**0.75**	0.625	Axial
	3-06	75	3.75	**3.25**	0.625	Axial
	3-07	75	***1.25***	2	0.625	Axial
	3-08	75	***6.25***	2	0.625	Axial
	3-09	75	3.75	2	0.625	Center
	3-10	75	3.75	2	0.625	Center

An additional scoping study (block zero), Table 4-3, was added to characterize the effects of the use of the HMWM primer at the bond line and between the reinforcement and concrete. These additional tests assessed if primer could be omitted in the larger test series and the results could support less stringent requirements when access and schedule make the application of primer impractical. A fractional factorial design (2^{3-1} – Resolution III) was used. Five specimens were cast without the HMWM primer along with five specimens with identical parameters with HMWM applied per manufacturer instructions.

Table 4-3. Scoping study experimental matrix

	Run	Temperature T (°F)	Splice length ℓ_s (in)	Side Cover c_b (in)	Bar diameter d_b (in)	Point Description
Batch/Block 0	0-01p	110	2.5	1.375	0.625	Primer
	0-01	110	2.5	1.375	0.625	No primer
	0-02p	40	2.5	2.625	0.625	Primer
	0-02	40	2.5	2.625	0.625	No primer
	0-03p	40	5	1.375	0.625	Primer
	0-03	40	5	1.375	0.625	No primer
	0-04p	110	5	2.625	0.625	Primer
	0-04	110	5	2.625	0.625	No primer
	0-05p	75	3.75	2	0.625	Primer
	0-05	75	3.75	2	0.625	No primer

4.2. CONCRETE

The cementitious concrete used as the stiffening strip for each specimen had a maximum aggregate size of 3/8 in. One batch of concrete was mixed per testing block. Compressive strength testing was completed 28 days after casting. Table 4-4 shows the average compressive strengths for each block.

Table 4-4. Cementitious concrete compressive strengths

Block #	Compressive Strength
0	5137 psi
1	3865 psi
2	4531 psi
3	4547 psi

4.3. DEFORMED BAR REINFORCEMENT

All reinforcing used in the material testing and non-contact splice testing were normal strength Grade 60 uncoated and epoxy-coated reinforcement. The reinforcement met ASTM A706 (ASTM 2022), with the coating meeting ASTM A775 (ASTM 2019). All bars were tested following ASTM A370 (ASTM 2020b). Two to four bars were tested for each bar size using a two-inch extensometer under two-stage displacement control. Stage one loaded the specimen at a rate of 0.15 in/min until the stress reached the estimated yield stress. Stage two loaded the specimen at a rate of 0.5 in/min until failure. During stage two, the extensometer was removed from the specimen prior to failure. Figure 4-3 shows one of the stress-strain curves for each bar size tested. Table 4-5 summarizes the average yield and tensile strengths for each bar. The yield strength for each test was determined using the 0.2% offset method.

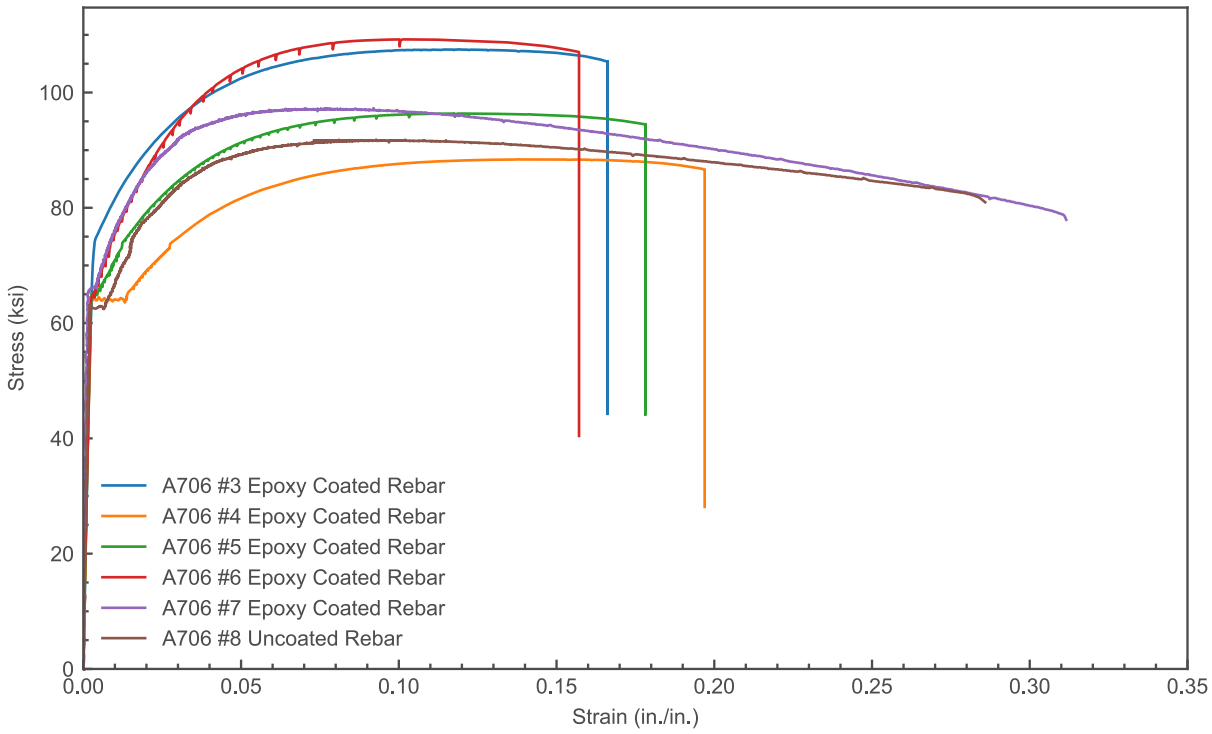

Figure 4-3. Tensile stress-strain response of epoxy-coated reinforcing bars

Table 4-5. Properties of reinforcing steel

Bar Size	Bar Coating	Bar Type	Avg Yield Strength (psi)	Avg Tensile Strength (psi)
No. 3	Epoxy	A706 Gr 60, A775	74900	107400
No. 4	Epoxy	A706 Gr 60, A775	64800	89000
No. 5	Epoxy	A706 Gr 60, A775	64500	96000
No. 6	Epoxy	A706 Gr 60, A775	66400	109200
No. 7	Epoxy	A706 Gr 60, A775	66600	97400
No. 8	Uncoated	A706 Gr60	66900	92700

4.4. POLYMER CONCRETE

The same HCSC mix ratios used in the mechanical characterization testing were used for the non-contact splice tests. All blocks were poured with one mixed batch, with approximately 230 lbs of prebagged aggregate and basalt fiber mix. The same mixing and casting procedure was used for the HCSC portion of the non-contact splice specimens with HMWM primer being applied as described in Section 3.3.

Compressive strength testing was completed at the midpoint of testing for each group of temperatures for each batch. Table 4-6 shows the compressive strengths of each batch. Three compressive cylinders were tested for each batch at each temperature. Batch 3 contained star points with extreme cold and hot temperatures.

Table 4-6. HCSC compressive strengths

Type	Block #	Age of specimen (days)	Average Temperature (°F)	Average Compressive Strength (psi)
Room	0	7	71.4	9395
	1	12	71.4	9241
	2	12	71.0	9591
	3	7	75.3	9250
Hot	0	18	120.4	5600
	1	13	116.1	5681
	2	14	117.7	5245
	3	11	157.7	1756
Cold	0	18	41.2	11664
	1	14	23.6	13002
	2	17	37.7	11883
	3	11	11.7	12724

4.5. CONSTRUCTION SEQUENCE

Non-contact splice specimens were completed in a two-part casting sequence. The procedure is broken down below:

1. Assemble 3/4 in MDO plywood forms with single-sided threaded uncoated rebar. One group form per depth per batch. Coat the bond line between the cementitious concrete and polymer concrete with a surface retarder for an exposed aggregate finish, Figure 4-4a.
2. Mix and pour cementitious concrete into forms. Smooth finish with a trowel, cover with wet burlap and plastic sheeting, and cure for 7 days, Figure 4-4b.
3. Demold cementitious concrete specimens and prepare bond line by pressure washing retarder and excess aggregate, Figure 4-4c.
4. Assemble 3/4 in melamine forms to full specimen size around the existing concrete specimen, Figure 4-4d.
5. Follow the mixing and fabrication procedure outlined in Section 3.3 and Section 3.4

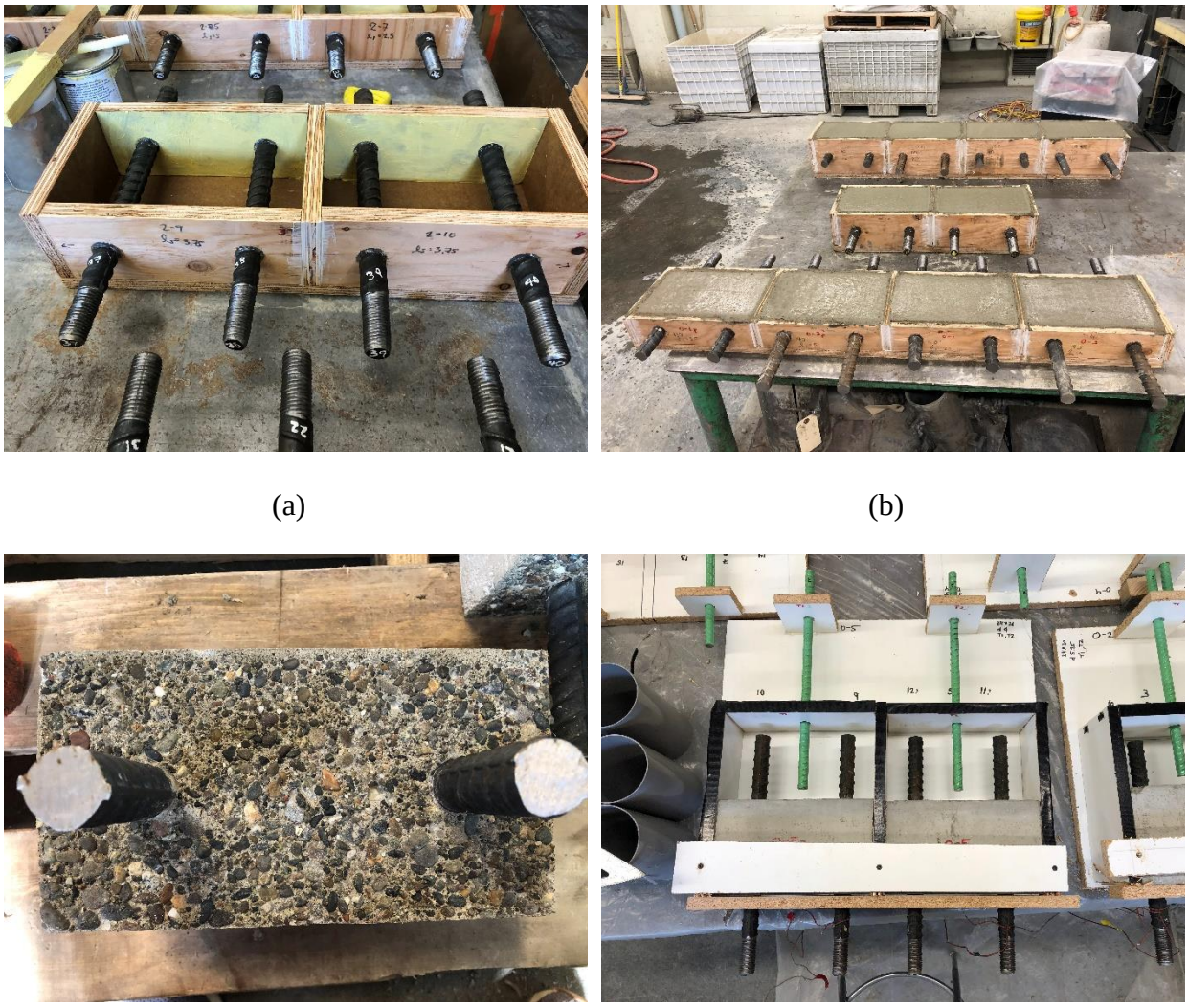

(a) (b)

(c) (d)

Figure 4-4. Non-contact splice specimen casting procedure: (a) cementitious concrete formwork, (b) cast cementitious concrete, (c) exposed aggregate finish, (d) HCSC formwork

4.6. TEMPERATURE DURING CONDITIONING

Once demolded and cured for 7 days under ambient conditions, the specimens were conditioned to the target test temperatures. The specimens were kept in the temperature-controlled cabinets for at least 16 hours prior to testing to achieve the desired internal temperature, monitored by embedded thermocouples in the specimens. Figure 4-5 shows the internal temperature change for

non-contact splice specimens during the conditioning period. The dashed lines indicate the temperature of the chamber.

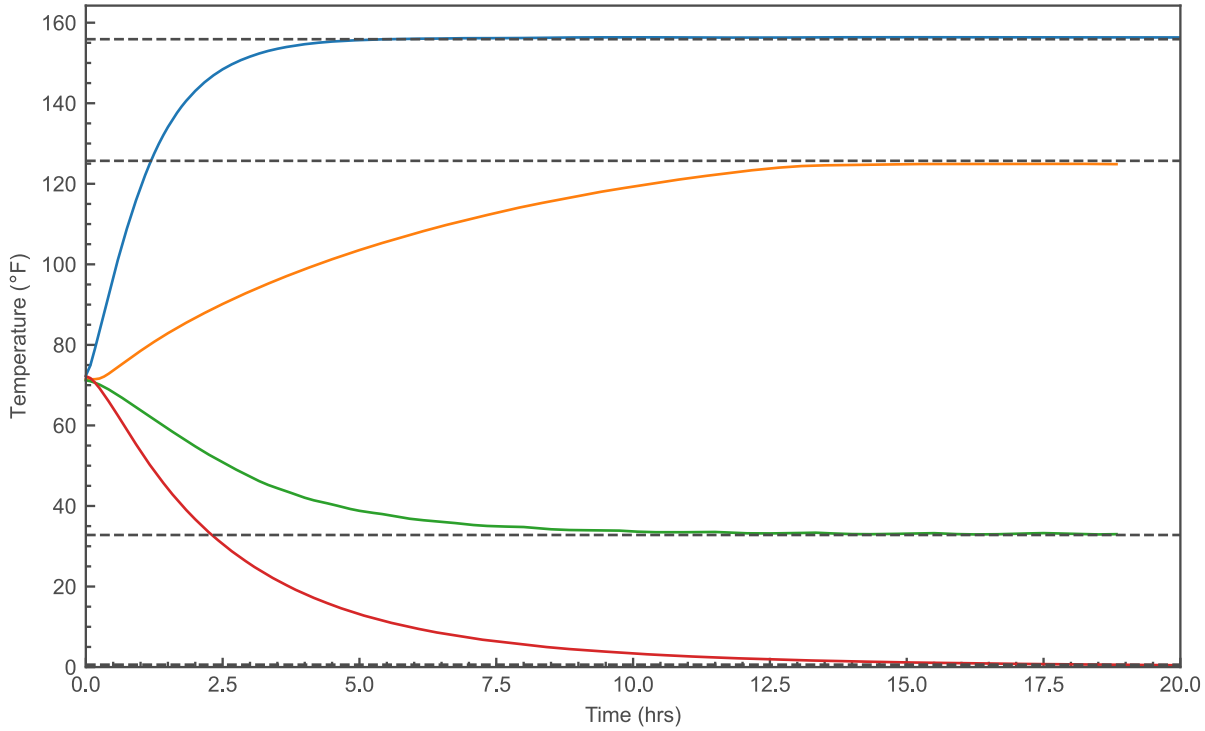

Figure 4-5. Temperature of non-contact splice specimens during curing

4.7. INSTRUMENTATION

Non-contact splice tests were conducted in an Instron Universal Testing Machine (UTM) with a capacity of 130,000 lbf. For each test, test time, applied load, and crosshead displacement over the duration of the test were recorded by the UTM. Figure 4-6 shows the additional instrumentation that was added to the UTM and specimens. The added instrumentation connected to a data acquisition system (DAQ) to record additional displacements and temperatures and allow for syncing between data during analysis.

To track the internal temperature of specimens during the casting, curing, and testing process, Type J thermocouples were embedded in the HCSC portion of the specimen, at approximate mid-depth.

During the casting and curing process, the temperature was recorded at five-minute intervals. An additional thermocouple was kept exposed to record the ambient temperature of the laboratory. To determine the change in temperature throughout the test, the temperature was also recorded during testing at a frequency of 10 Hz.

LVDTs arranged at 180 degrees to each other were attached to the epoxy-coated rebar four inches above the face of the specimen to record the slip displacement of the reinforcement relative to the top face of the HCSC. One LVDT was added to the crosshead of the UTM to record the movement of the crosshead. This allowed for the displacements of the rebar slip and UTM crosshead to be synced. LVDT measurements were recorded at a frequency of 10 Hz.

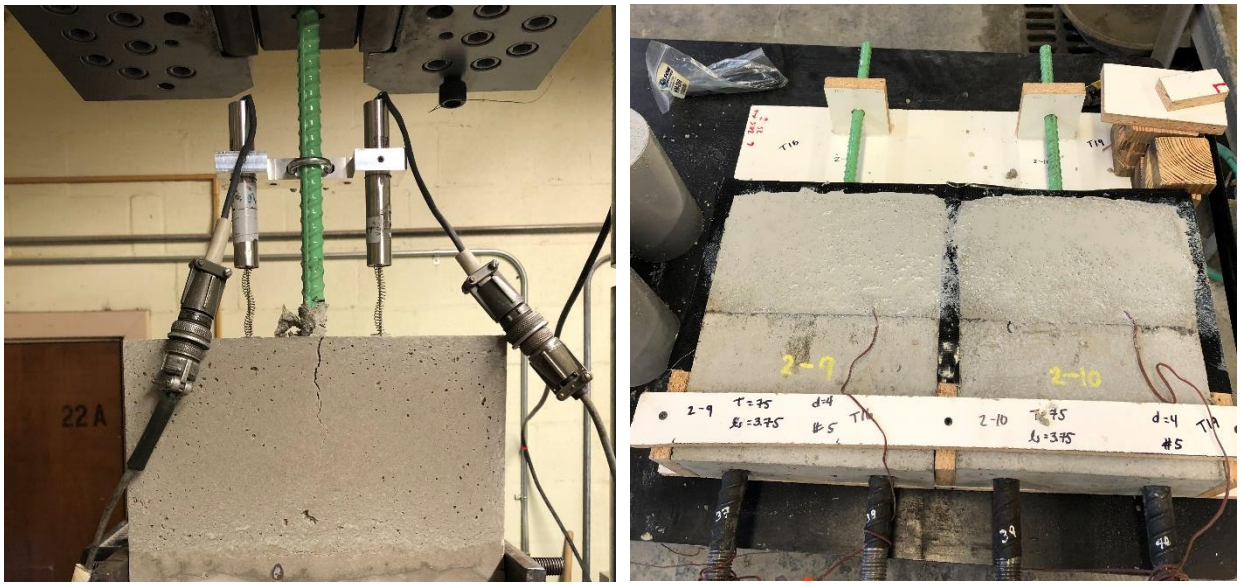

(a) (b)

Figure 4-6. (a) LVDT placement on reinforcement, (b) embedded thermocouples

4.8. TEST PROCEDURE

Testing was conducted by applying monotonically increasing vertical displacements to the free ends of the reinforcement and measuring the resulting loads using the test machine's internal load cell. The two No. 8 anchorage bars were threaded at their ends and were used to connect the specimens to the bottom platen of the testing machine, which remained fixed, Figure 4-7. The free end of the epoxy-coated reinforcement was gripped in the top jaws of the testing machine. The tension load was applied under closed-loop displacement control at a constant rate of 0.2 in./min. Two LVDTs arranged 180 degrees opposite one another were attached to the epoxy-coated rebar to record the slip displacement of the reinforcement relative to the top face of the HCSC. To prevent damage to the instrumentation and test machine when the specimen failed, the concrete strip was restrained transverse to the axis of the splice using exterior steel plates and four 0.5 in diameter threaded rods. The rods were hand tightened before starting the tests, providing minimal restraint against splitting at the top surface of the specimen.

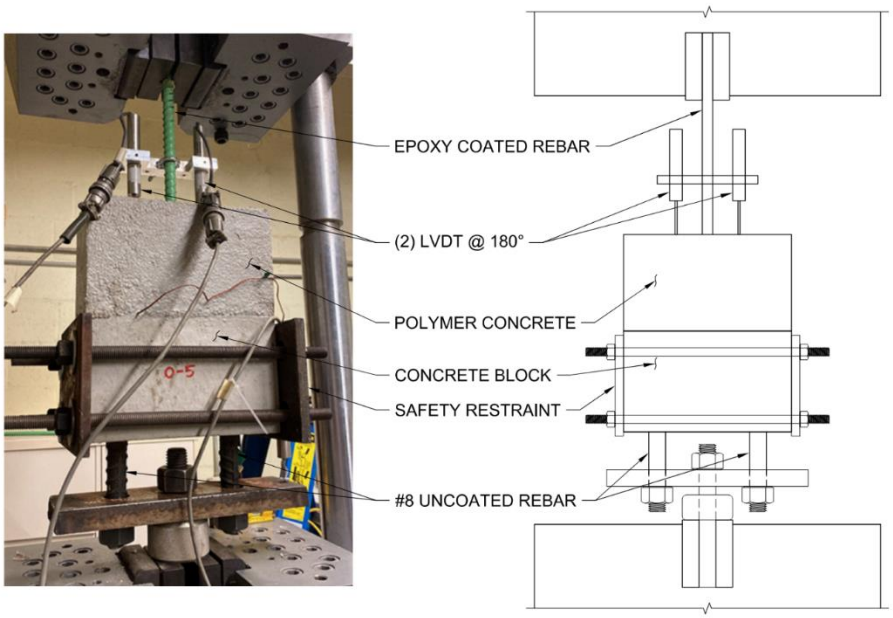

Figure 4-7. Non-contact splice testing setup

4.9. TEMPERATURE DURING TESTING

During testing, the specimens were individually removed from the conditioning chamber and promptly tested to reduce deviation from the target test temperatures. Table 4-7 shows the average surface and internal temperature for each testing temperature. The rate of temperature change varies at high and low temperatures.

Table 4-7. Average surface and internal temperature during testing

Type	Target Temp. (°F)	Avg. Surface Temp. (°F)		Avg. Internal Temp. (°F)	
		Start	End	Start	End
Cold, n = 8	40	44.0	46.5	30.4	32.0
Hot, n = 8	110	116.6	115.6	118.6	118.0
Coldest, n = 1	5	14.7	17.4	1.4	4.0
Hottest, n = 1	145	155.8	151.8	155.7	153.6

Figure 4-8 shows the internal and surface temperature for two specimens with identical splice length, side cover, and bar size. While the testing duration varied between tests, a larger temperature change was observed for specimens tested at low temperatures, indicating different rates of heat flow.

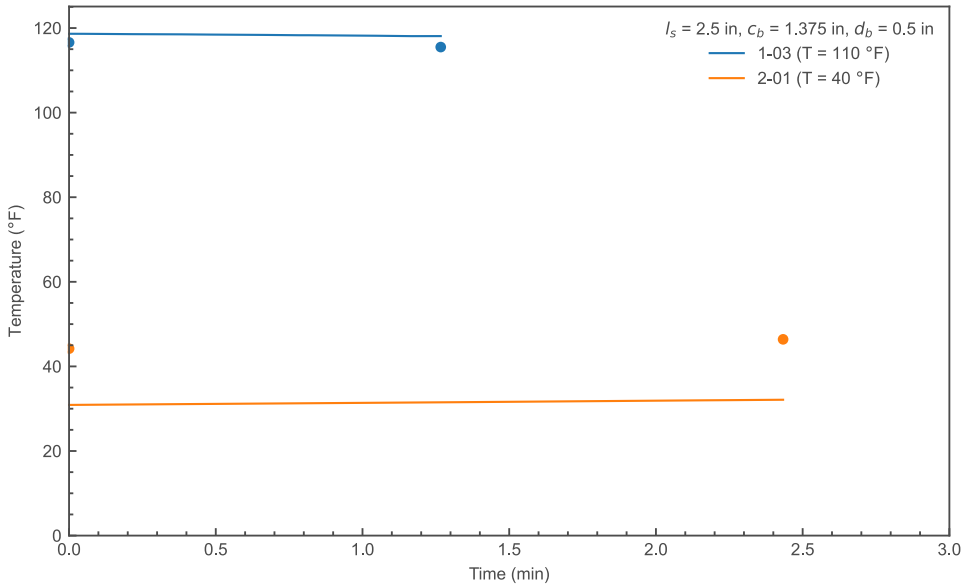

Figure 4-8. Internal and surface specimen temperature for similar specimens

CHAPTER 5. RESULTS

Table 5-1 summarizes the results of the non-contact splice tests for the scoping study and CCD design.

Table 5-1. Summary of experimental testing results

	Run	Point Description	Observed Failure	Max Load (lb)	Bar Stress (ksi)
Block/Batch 0 (Scoping Study)	0-01p	Primer	Splitting	12419	40.06
	0-01	No primer	Splitting	11136	35.92
	0-02p	Primer	Splitting	25086	80.92
	0-02	No primer	Splitting	22760	73.42
	0-03p	Primer	Splitting	23071	74.42
	0-03	No primer	Splitting	19844	64.01
	0-04p	Primer	Splitting	26157	84.38
	0-04	No primer	Splitting	25722	82.97
	0-05p	Primer	Splitting	24524	79.11
	0-05	No primer	Splitting	22313	71.98
Block / Batch 1	1-01	Factorial	**Bar Fracture**	17433	87.17
	1-02	Factorial	**Bar Fracture**	17494	87.47
	1-03	Factorial	Splitting	12103	60.52
	1-04	Factorial	**Bar Fracture**	17082	85.41
	1-05	Factorial	Splitting	17225	39.15
	1-06	Factorial	Splitting	42262	96.05
	1-07	Factorial	Splitting	21422	48.69
	1-08	Factorial	Splitting	19222	43.69
	1-09	Center	Splitting	26561	85.68
	1-10	Center	Splitting	25625	82.66
Block / Batch 2	2-01	Factorial	Splitting	14655	73.28
	2-02	Factorial	**Bar Fracture**	17426	87.13
	2-03	Factorial	Splitting	15201	76.01
	2-04	Factorial	**Pullout**	14159	70.80
	2-05	Factorial	Splitting	24165	54.92
	2-06	Factorial	Splitting	29765	67.65
	2-07	Factorial	Splitting	13765	31.28
	2-08	Factorial	Splitting	30539	69.41
	2-09	Center	Splitting	24481	78.97
	2-10	Center	Splitting	25245	81.44
Block / Batch 3	3-01	Axial	**Bar Fracture**	11443	104.03
	3-02	Axial	Splitting	30437	50.73
	3-03	Axial	Splitting	*29534*	*95.27*
	3-04	Axial	**Pullout**	***7062***	***22.78***
	3-05	Axial	Splitting	14342	46.26
	3-06	Axial	**Bar Fracture**	29646	95.63
	3-07	Axial	Splitting	15366	49.57
	3-08	Axial	**Bar Fracture**	29503	95.17
	3-09	Center	Splitting	25417	81.99
	3-10	Center	Splitting	25131	81.07

5.1. INFLUENCE OF PRIMER

All specimens in the scoping study (batch 0) failed through a bond splitting mechanism as designed, Figure 5-1. All specimens with primer exhibited larger bar stresses at failure than those without primer. Table 5-2 summarizes the percent change in bar stress due to HMWM primer usage, with positive values indicating larger stress in specimens with primer.

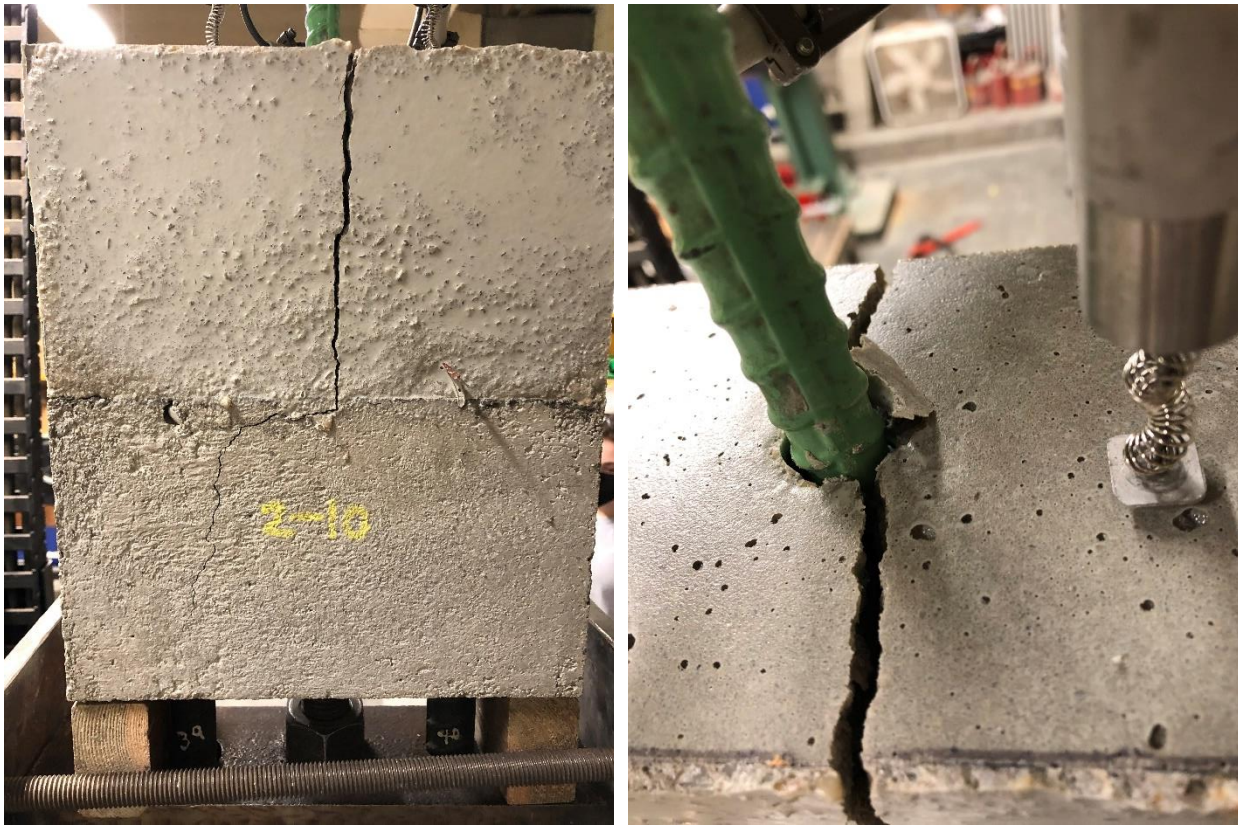

(a) (b)

Figure 5-1. (a) Elevation view of splitting failure, 2-10, (b) Splitting at top of HCSC, 2-10

Table 5-2. Percent change in bar stress due to HMWM primer usage

Run	Bar Stress (ksi)
0-01p/0-01	10.33%
0-02p/0-02	9.27%
0-03p/0-03	13.99%
0-04p/0-04	1.66%
0-05p/0-05	9.02%
Average	8.85%

Due to using a fractional factorial design (2^{3-1} – Resolution III), confounding occurs with two-factor interactions. However, the main effects are not aliased with each other so a main effects plot can be created to determine how each parameter affects the bar stress response. Minitab, a statistical analysis software, was used to analyze the results of the non-contact splice tests (Minitab 2022). To create the main effects plot, equations for bar stress were created using the trends found in the factorial points (runs 0-1 through 0-4) for each parameter (splice length, side cover, and temperature). These equations were then plotted across the range of the parameter.

Figure 5-2 shows the main effects of the specimens with and without the use of HMWM primer. The blue line shows the bar stress response for the range of the factorial points. The red dot is the measured center point data. Measured data for the cast specimens was used for the analysis. For both types of specimens, bar stress increased as splice length and side cover were increased. This relationship between the bar stress at failure is similar to that observed in normal strength, cementitious concrete. The decrease in bar stress with increases in testing temperature is consistent with the relationship between HCSC strength and temperature from the mechanical characterization testing. The same trends are found in the main effects plot for the specimens with HMWM primer.

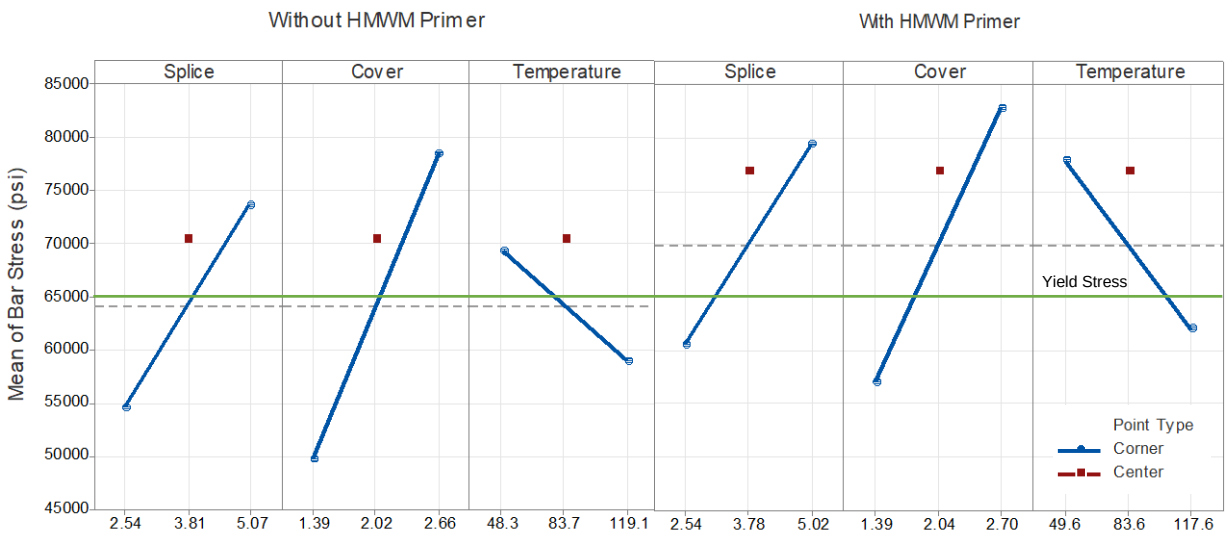

Figure 5-2. Main effects of usage of HMWM primer

The bar stress for the tests with and without HMWM primer is above bar yield for the center point of the design space. There is a vertical shift between the two main effects plots indicating that the usage of primer does affect the observed bar stress. The overall mean of bar stress for specimens without HMWM primer was 64.1 ksi while specimens with HMWM primer had an average of 69.9 ksi, a 9% increase in bar stress. The use of HMWM primer is recommended based on the testing results and by the manufacturer. The usage of primer would allow for smaller joint widths due to reducing splice length and cover requirements to reach bar yielding.

5.2. INFLUENCE OF TEMPERATURE, SPLICE LENGTH, AND BAR COVER

Figure 5-1, Figure 5-3, and Figure 5-4 show the failure patterns that were observed in the test program. The majority of specimens failed through a bond splitting mechanism, as designed. The remainder failed through fracturing of the embedded reinforcement, Figure 5-3, or through a pullout mechanism, Figure 5-4. Fracture of the reinforcement was observed at the extremities of the experimental design space as expected, at lower test temperatures, longer splice lengths, larger side covers, and smaller bar diameters when compared to the center of the design space

(a) (b) (c)

Figure 5-3. (a) Elevation view of bar fracture, 1-02, (b) Rebar at top of HCSC, 1-02, (c) Bar fracture and top of HCSC, 1-04

(a) (b)

Figure 5-4. (a) Elevation view of pullout failure, 2-04, (b) Pullout at top of HCSC, 2-04

5.2.1. Batch-to-Batch Variability

Table 5-3 compares the measured bar stress at failure for the six nominally identical center point specimens (for reference the yield and ultimate strength of the reinforcement were 65.0 ksi and 96.0 ksi, respectively). Because the experimental design was conducted using three separate batches of HCSC, an important consideration was the batch-to-batch variability of the repeated center point. In each batch, two specimens were tested with identical properties, the center point of the design space (T =75 °F, ℓ_s = 3.75 in, c_b = 2.0 in, and d_b = 0.625 in). This comparison also considers the inherent variability between specimens due to small construction, conditioning, and testing differences. The strength of the CCD design is the ability to quantify and incorporate this variability in analyzing the experimental results. The very low coefficient of variation between the six specimens (<5%) shows that the batch-to-batch variation was small.

Table 5-3. Bar stress at failure for repeated center point specimens

Run	**Bar Stress (ksi)**
1-09	85.7
1-10	82.7
2-09	79.0
2-10	81.4
3-09	82.0
3-10	81.1
Mean	82.0
Standard Deviation	2.2
Coeff. Of Variation	2.7 %

5.2.2. Stress-Slip Behavior

Two star points, one high and one low, were tested for each parameter. Each start point had one high or low parameter with all other parameters kept at the center point. These star points are compared to the center point specimens in Figure 5-5, Figure 5-6, and Figure 5-7. For all plots, the equivalent stress-slip curve of a #5 epoxy-coated rebar was plotted. This curve is an adaptation from the tested stress-strain curve of the reinforcement. The LVDTs placed on the non-contact splice specimens were located four inches above the face of the polymer concrete. Therefore, the strain from the reinforcement curve can be modified to plot rebar displacement with respect to stress. This line represents the displacement of the rebar without any bond slip. When analyzing the plots, the difference between the reinforcement curve and the measured response is indicative of the slip due to bond.

The temperature star points (5 °F and 145 °F) show the range in strength of HCSC at high and low temperatures, Figure 5-5. For the specimen tested at a low temperature, a small yield plateau and high bar stress at failure was observed. The stress-strain curve is stiffer than the center point and has high bond strength, shown by the small difference between the curve of the reinforcement and the specimen. It is important to note that the behavior is of the composite specimen, not HCSC individually. Though the observed failure method observed was splitting, the bar stress was 95.3 ksi, very close to the tensile strength of the bar. The specimen tested at a high temperature did not reach bar yield and is much less stiff than the center point. The behavior is a ductile failure method of bar pullout.

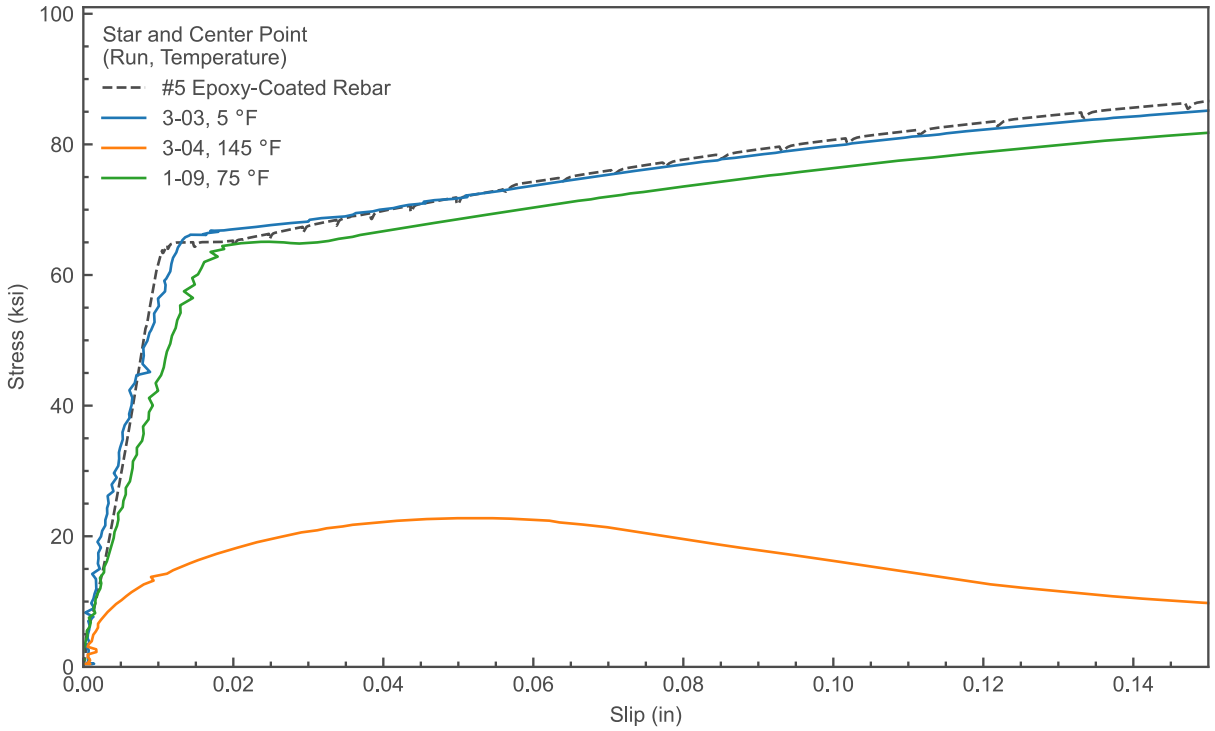

Figure 5-5. Stress-front end displacement for temperature star points and center points

Figure 5-6 and Figure 5-7 show the star points for splice length (1.25 in. and 6.25 in.) and side cover (0.75 in. and 3.25 in.), respectively. The extreme low parameters for both splice length and side cover exhibit similar behavior. Both specimens with minimal splice length or side cover failed via splitting with bar stresses below yield. The stiffness of the specimens was similar to the center points, until close to failure. The stress-strain behavior is quite brittle, due to the poor confinement and lack of capability for bond development. The specimens with large splice length or side cover both failed due to bar fracture. Sufficient bond could be developed such that the specimens could withstand loading larger than the tensile strength of the reinforcement. The stress-strain curves have similar stiffnesses and yield plateaus compared to the center point.

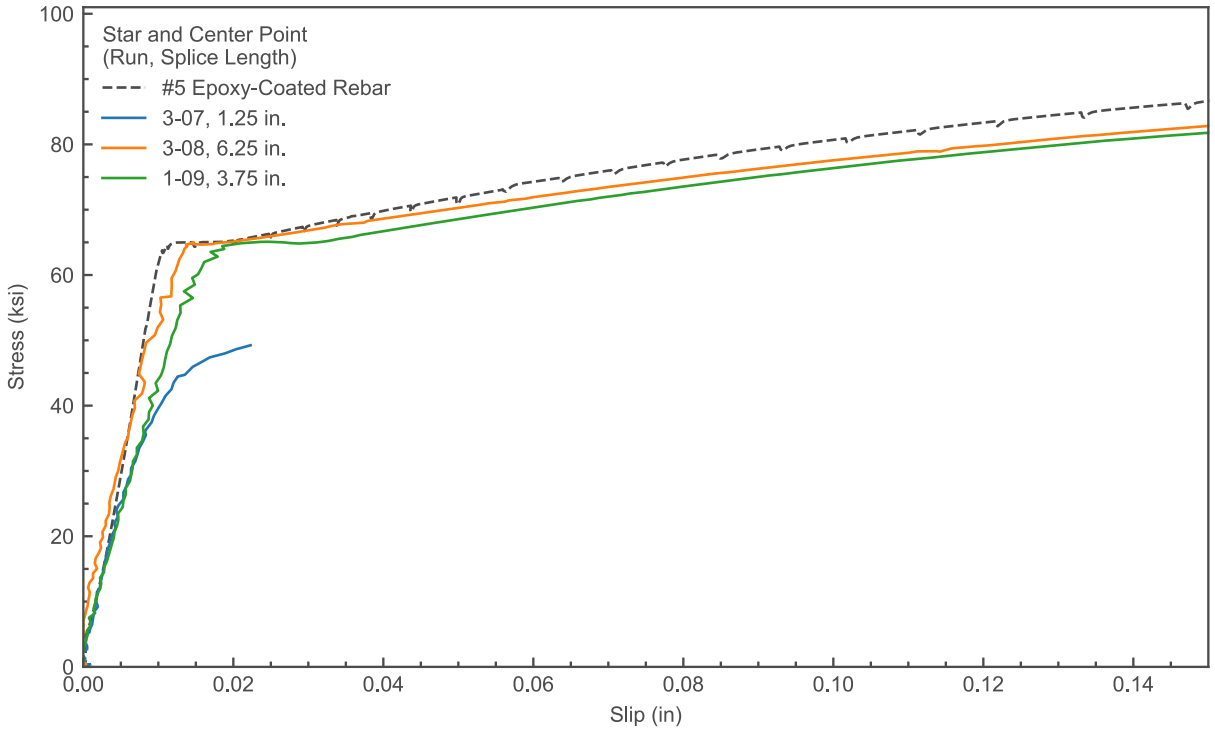

Figure 5-6. Stress-front end displacement for splice length star points and center points

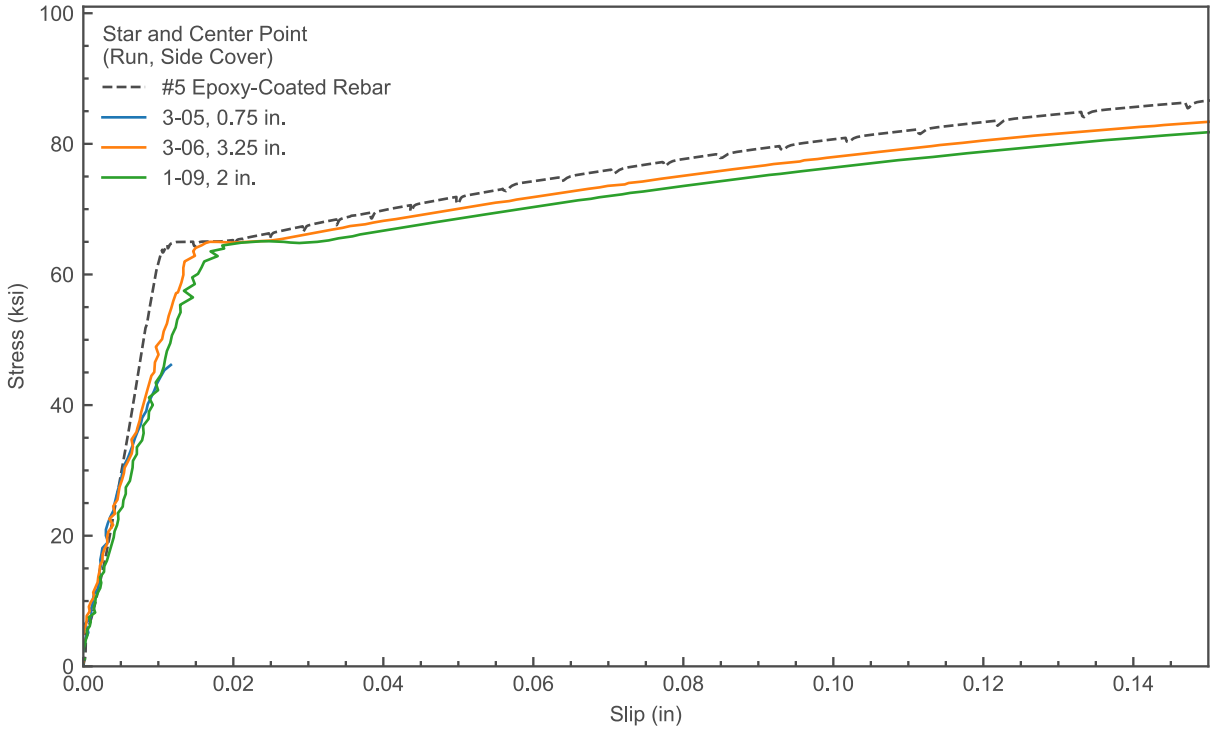

Figure 5-7. Stress-front end displacement for side cover star points and center points

Figure 5-8 shows the star points for bar diameter (0.375 in. and 0.875 in.) The star points for bar diameter affect the load that can be applied to the specimen before bar failure and also change the bond characteristics as the splice length and side cover in terms of the number of bar diameters changes. The specimen with a #3 bar (0.375 in diameter) failed due to bar fracture with extremely ductile behavior. There is no yield plateau and similar stiffness to the center points. Sufficient bond strength is developed due to large splice lengths and side cover with respect to the bar diameter, resulting in a force large enough to exceed the ultimate strength of the rebar. The specimen with a #7 bar (0.875 in diameter) failed due to brittle splitting of the specimen. The bar stress at failure was below the yield stress of the rebar. The large cross-section area of the reinforcement resulted in large forces being applied to the specimen. When compared to the bar diameter, the splice length and side cover were small, so poor confinement of the bar led to radiating stresses from the bar reaching the edges of the specimen, resulting in cracking and eventually splitting failure.

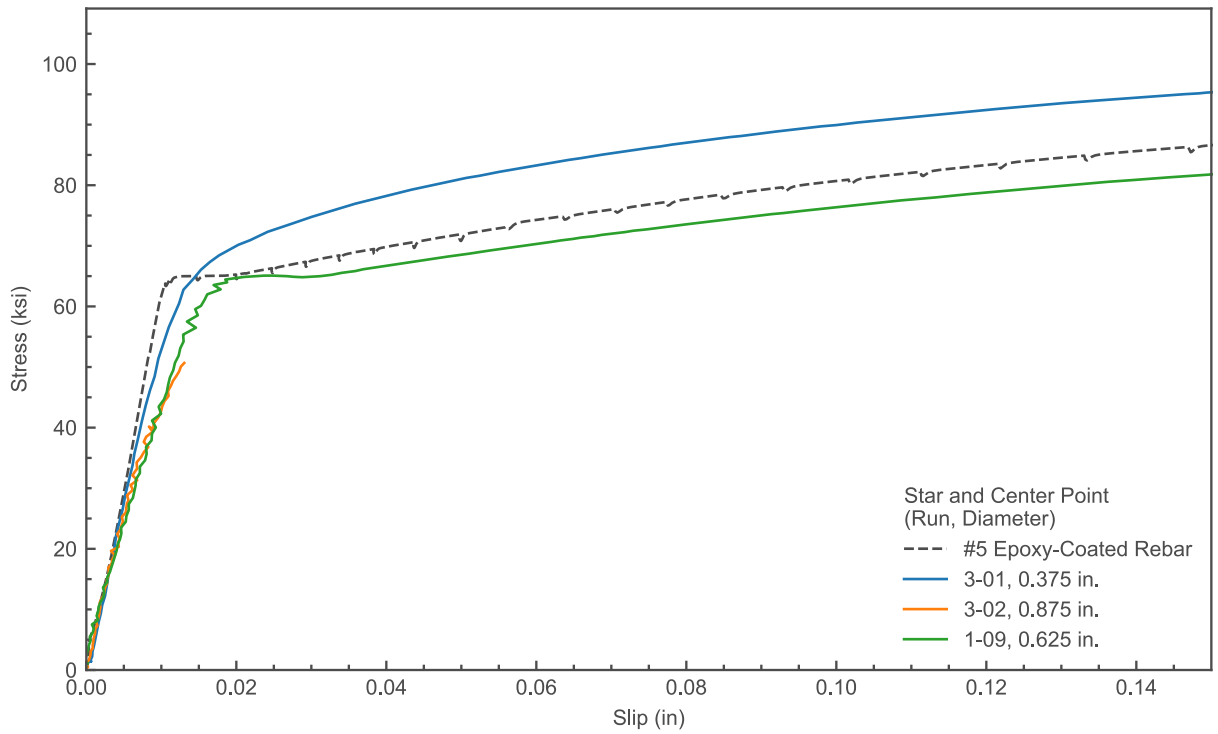

Figure 5-8. Stress- front end displacement for bar size star points and center points

5.2.3. Maximum Bar Stress

Figure 5-9 compares the normalized splice length in terms of the number of bar diameters and bar stress for the main specimens in the non-contact splice tests. Temperature is shown based on the color of the marker. Only specimens with greater than three bar diameters of cover are shown. Additional points are plotted for a non-proprietary UHPC mix. For increasing splice lengths, the bar stress increases, eventually resulting in bar fracture once stresses in the specimen exceed the ultimate strength of the reinforcement. Specimens tested at colder temperatures failed at higher bar stressed for the same splice length. The bar stresses of the reinforcement embedded in HCSC are comparable to those in UHPC indicating similar bond performance. Specimens with splice lengths larger than five bar diameters failed above bar yield.

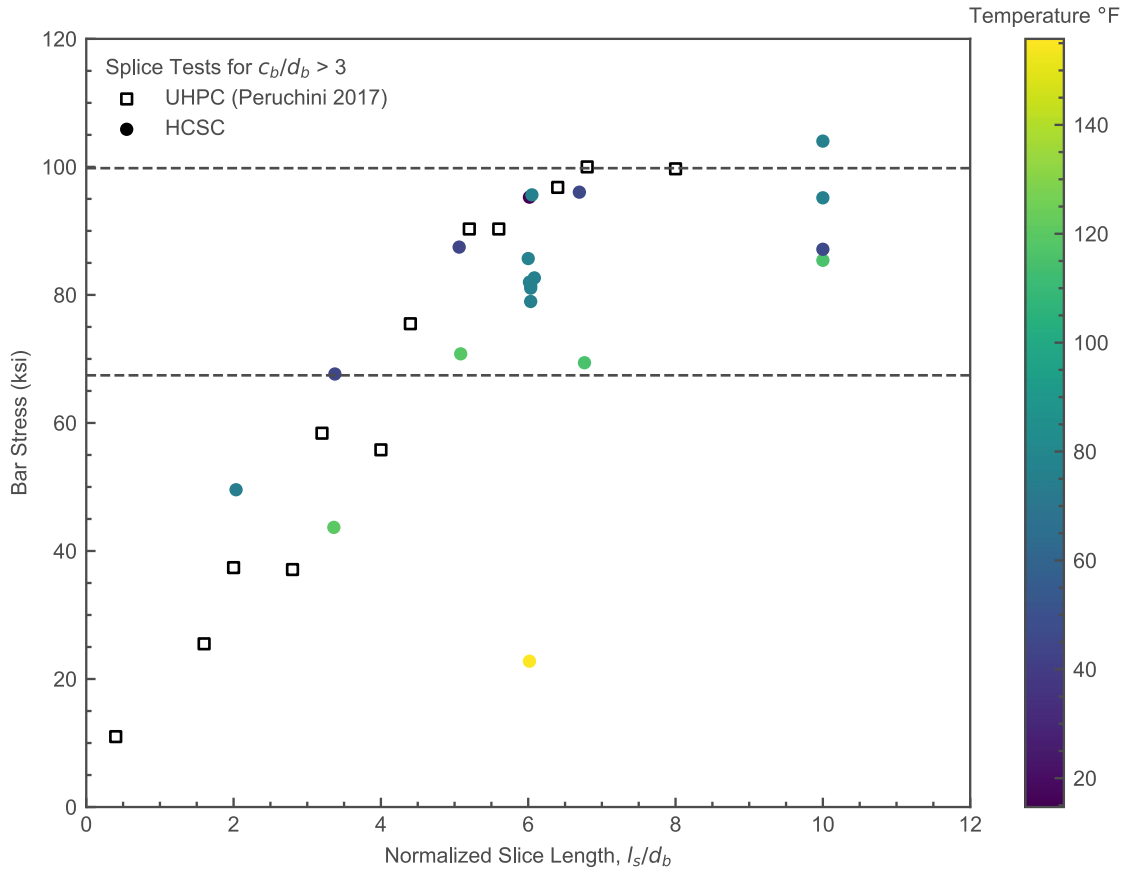

Figure 5-9. Comparison of normalized splice length and bar stress

Using the measured geometry of each specimen and the measured surface temperature at the start of testing, a regression analysis was performed in Minitab for the non-contact splice specimens. Analysis of variance testing (ANOVA) and response surface methodology (RSM) were used to create a model to explore the relationship of parameters with bar stress and other testing parameters.

The four-factor CCD design allows for linear, square, and two-way interaction terms. Table 5-4 shows the initial model with all combinations of terms and the terms that were included in the final model, which was reduced to only include significant terms. The final equal to model bar stress is shown at the bottom of the table. F-values and P-values were used to determine each term's significance. Terms with large P-values were removed from the model as the null hypothesis of a

term being statistically insignificant can be rejected. Though P-values are typically kept below a significance level of 0.05, some terms were kept in the selected model terms to prevent entire term types (linear, square, or two-way interaction) from being excluded from the model. Additionally, terms were retained to capture the physical phenomena that were observed in both material characterization and during non-contact splice testing.

Table 5-4. Analysis of Variance Results

Source	All Terms		Selected Terms	
	F-Value	P-Value	F-Value	P-Value
Model	10.99	0.00004	18.70	0.00000
Blocks	0.33	0.72300	0.38	0.68931
Linear	37.49	0.00000	45.77	0.00000
Temperature (T)	44.34	0.00002	52.19	0.00000
Bar Diameter (d_b)	48.89	0.00001	58.36	0.00000
Splice Length (ℓ_s)	28.91	0.00013	35.12	0.00001
Side Cover (c_b)	30.67	0.00010	40.06	0.00001
Square	4.23	0.02067	6.32	0.00407
Temperature * Temperature	13.76	0.00262	15.59	0.00094
Diameter*Diameter	0.98	0.34074	-	-
Splice Length*Splice Length	3.08	0.10272	3.13	0.09367
Side Cover*Side Cover	3.65	0.07826	3.65	0.07224
2-Way Interaction	1.30	0.32281	3.88	0.03970
Temperature*Diameter	0.45	0.51341	-	-
Temperature*Splice Length	0.12	0.73138	-	-
Temperature*Side Cover	0.59	0.45444	-	-
Diameter*Splice Length	1.77	0.20570	2.06	0.16847
Diameter*Side Cover	4.80	0.04729	5.77	0.02726
Splice Length*Side Cover	0.00	0.97652	-	-

$$BarSress = 136113 + 466\mathrm{T} - 287725 d_b + 8899 \ell_s + 7841 c_b - 4.59 T^2 - 1663 \ell_s{}^2 - 7148 c_b{}^2 + 17759 * d_b * \ell_s + 60473 * d_b * c_b$$

The model was then used to create the main effects plot, Figure 5-10, and the interaction plot, Figure 5-11, for each parameter and its associated interactions. The main effect plot created for the CCD analysis is based on the bar stress model as opposed to the individual data points. The trends

in the CCD main effects plot are similar to the results from the scoping study, however, there is curvature in the trend lines due to higher order terms being included in the bar stress model.

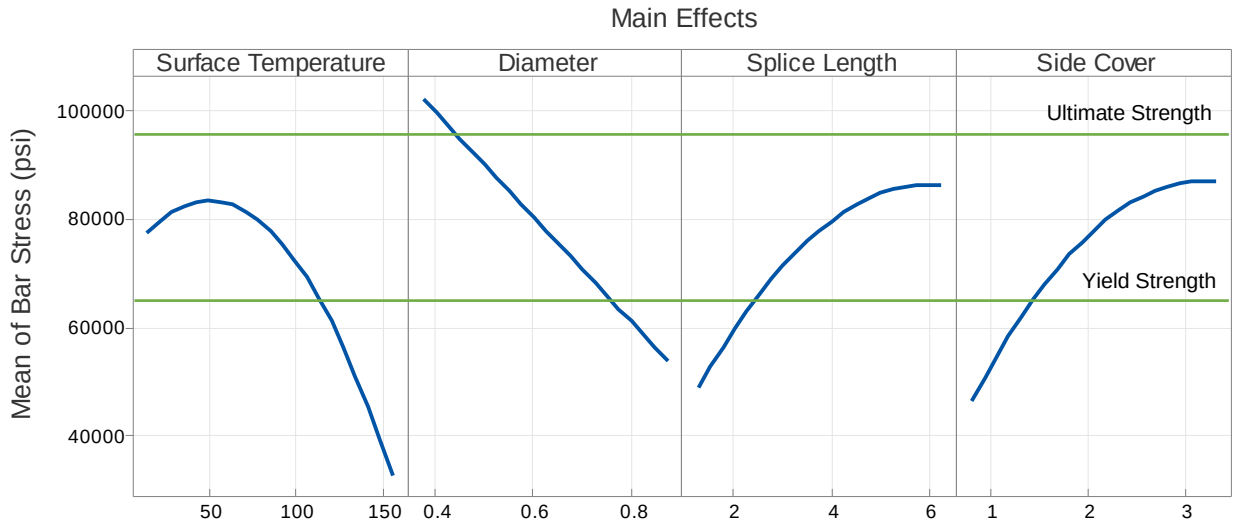

Figure 5-10. Main effects of CCD analysis

Similar to the mechanical characterization and the scoping study, larger bar stresses and material strengths are found at lower temperatures as the HCSC strengths are higher. At hotter temperatures, the material strength and bar stresses are reduced.

The parabolic shape for the surface temperature attempts to capture the change in material strength as a function of testing temperature. From the material characterization, it was observed that the material and therefore the achievable bar stress are lower at higher temperatures. This behavior is seen in the portion of the main effects plot greater than 50 °F. For lower temperatures, the reduction in bar stress is non-physical, i.e., it occurs due to inaccuracies in the model as opposed to physical represented phenomena. It was observed that the bar stress at failure plateaus once sufficiently low testing temperatures are reached.

The square term of diameter was removed from the model, resulting in the linearity of the effect of diameter on bar stress. As expected, increases in splice length and side cover result in larger bar stresses at specimen failure. Once sufficient cover and splice length are used, the bar can only develop stress until the ultimate strength of the bar is reached. Once the bar fractures additional cover or splice length has the same maximum stress (i.e., f_u). This results in the tapering of the curves in the plot as the bar stress approaches the ultimate strength.

The interaction diagram, Figure 5-11, displays the two-way interaction terms and their effects on bar stress at failure. Each panel is broken up into the low, mean, and high parameter levels for one of the interactions. Interactions between splice length and side cover are not shown as the two-way interaction term was not included in the model due to a lack of statistical significance. Additionally, temperature has no significant terms for two-way reactions, so it is also not included as a panel in the interaction diagram.

The interaction between splice length and bar diameter shows that for increasing splice lengths, bar stresses increase and then taper at a sufficient bond for all diameters. This is attributed to the upper limit of the bar stress being reached. For all bar diameters, once ultimate strength is reached the specimen will fail due to bar fracture, thus limiting the maximum achievable bar stress. When looked at from a perspective of splice length or side cover normalized by bar diameter, the lines would be positioned such that as the normalized splice length increased the bar stress would continually increase until the ultimate strength of the bar is reached.

The interaction between bar diameter and splice length as well as bar diameter and cover show similar trends. For smaller diameters, bar stress is higher. This is consistent with the relationship between stress, force, and area. It can also be attributed to the accepted concept that bars of larger

diameter have less efficient bond strength compared to bars of smaller diameter. For increasing cover or splice length at the same diameter, bar stress increases. This is attributed to better confinement and thus more load development before failure (most likely splitting) of the specimen.

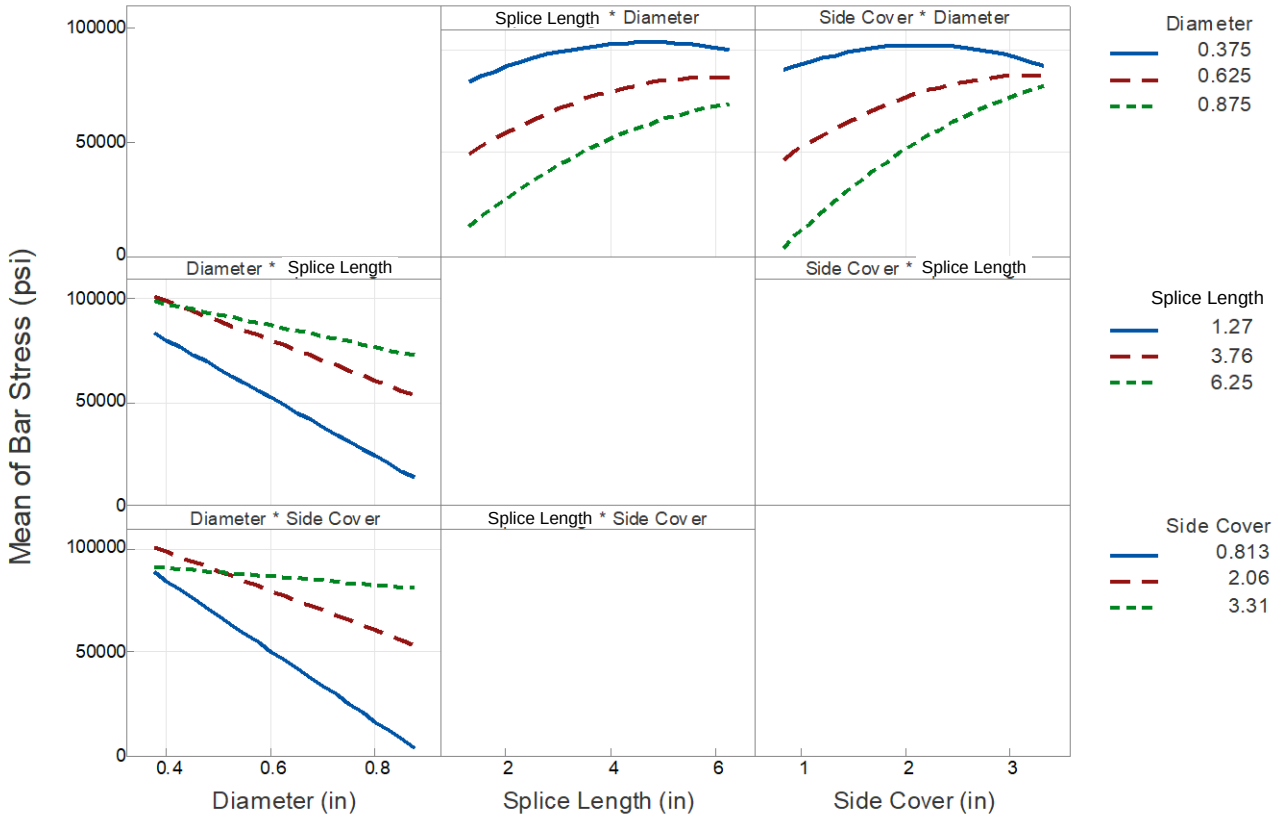

Figure 5-11. Interaction diagram of CCD analysis

CHAPTER 6. DESIGN RECOMMENDATIONS

6.1. CLOSURE JOINT GEOMETRY

In ABC, precast elements are often used to expedite project delivery, improve project quality, and reduce traffic disruptions. Once delivered on-site, adjacent precast superstructure elements are connected at closure joints. To complete the superstructure, the closure joints are filled with a field-cast material that creates continuity between the precast concrete elements by splicing the reinforcement protruding from the adjacent precast members within the joints. The geometry of the closure joints, the speed at which the connections can be completed, the curing time before the bridge can be opened to traffic, and the cost of the system are all dependent on the material that is used to fill the gaps between precast elements. Closure joint geometry is largely determined by the strength of closure pour material, particularly bond strength. Potential alternatives considered here include conventional cementitious concrete, UHPC, and HCSC.

Figure 6-1 shows an example joint geometry and reinforcement for a conventional cementitious concrete closure pour. This detail could be used for both transverse longitudinal joints. A minimum joint width of 12 in is specified by AASHTO. This width allows for adequate development of bonding between the concrete and reinforcement. The AASHTO LRFD Bridge Construction Specifications require vertical joints to be keyed. The preparation of the joint is important to ensure an adequate bond, typically an exposed aggregate finish. Additionally, the concrete in the closure joint should have the strength comparable to the precast components (Section 5.14). Per Section 5.11, the AASHTO specified basic development, l_d, for #11 bars and smaller is $1.25 * A_b * f_y/\sqrt{f'_c}$ and no less than $0.4 * d_b * f_y$. The minimum splice length for reinforcement in tension is 12 in and no less than $1.0 * l_d$.

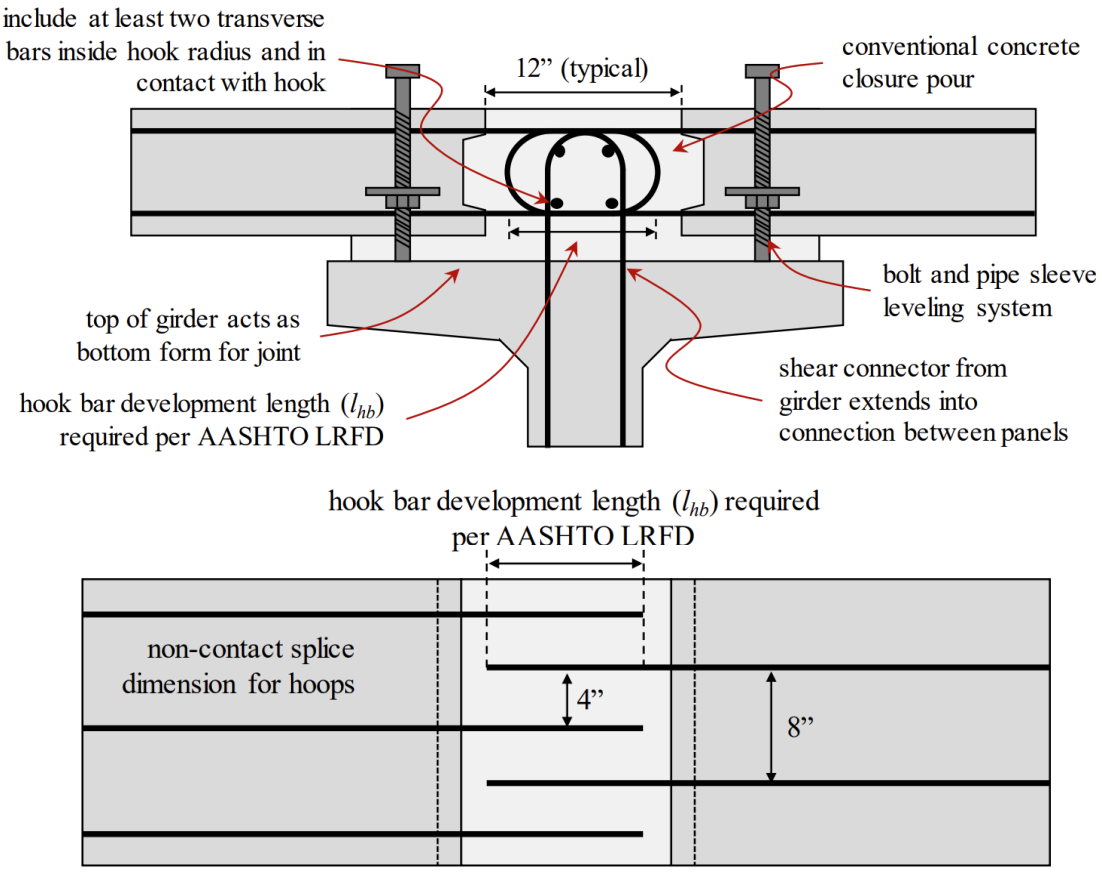

Figure 6-1. Conventional concrete closure joint per AASHTO specifications (Garber and Shahrokhinasab 2019)

Figure 6-2 shows an example of a UHPC closure joint detail. Research conducted by the FHWA (Graybeal 2014) provides guidance on the structural design of closure joints that have been adopted into the AASHTO LRFD Guide Specifications for Accelerated Bridge Construction (AASHTO 2018). This guidance recommends the minimum embedment length of deformed steel reinforcement, l_d, be taken as $8d_b$ for #8 bars or smaller with f_y less than or equal to 75 ksi. The embedment length recommendation requires that the cover be greater than or equal to $3d_b$ with UHPC having a compressive strength of at least 14 ksi and 2% fibers by volume. The splice length for straight deformed steel reinforcement is recommended to be at least $0.75l_d$, or $6d_b$ if an l_d of $8d_b$ is used. This results in a minimum joint width of $10d_b$ with some allowance for construction tolerance in the field.

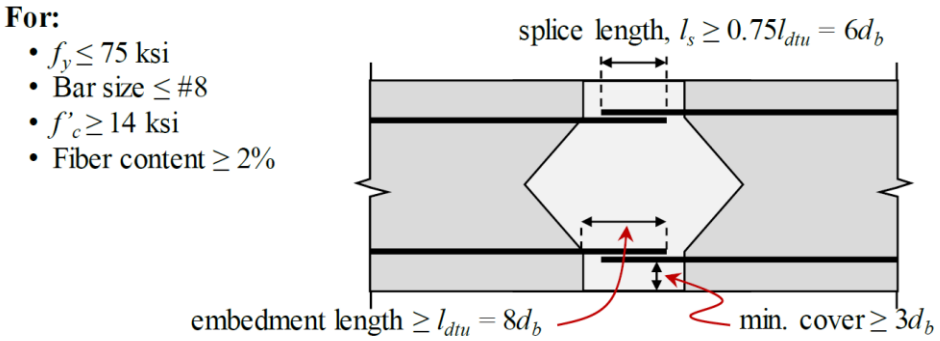

Figure 6-2. UHPC Recommended joint geometry (Garber and Shahrokhinasab 2019)

If HCSC in combination with HMWM primer is used, sufficient bond strength would be developed with the minimum AASHTO specified joint width, splice length, and development length. This however is impractical since HCSC is considerably stronger than conventional concrete and can thus be utilized in a more efficient joint geometry.

Instead, the material strengths should be used to determine the required joint width based on the bond strength the closure joint material provides. The parameters that influence bond strength are the material properties, splice length, side cover, bar size, and for PCs, temperature. The materials assumed to be used in this discussion are HCSC and epoxy-coated reinforcement, identical to the tested specimens. Since multiple parameters were changed for each specimen during testing, selecting a specimen to be used as a prototype geometry would not necessarily isolate the most efficient combination of parameters. Instead, Figure 6-3 shows a combination of testing temperature, bar size, splice length, and side cover based on the model created from the statistical analysis. The black dashed line denotes the yield strength, and the grey line denotes the ultimate strength of the reinforcement. The white dashed line shows the UHPC closure joint design recommendation by the FHWA (Graybeal 2014). The design area is the upper right corner, in which sufficient cover and splice length is provided.

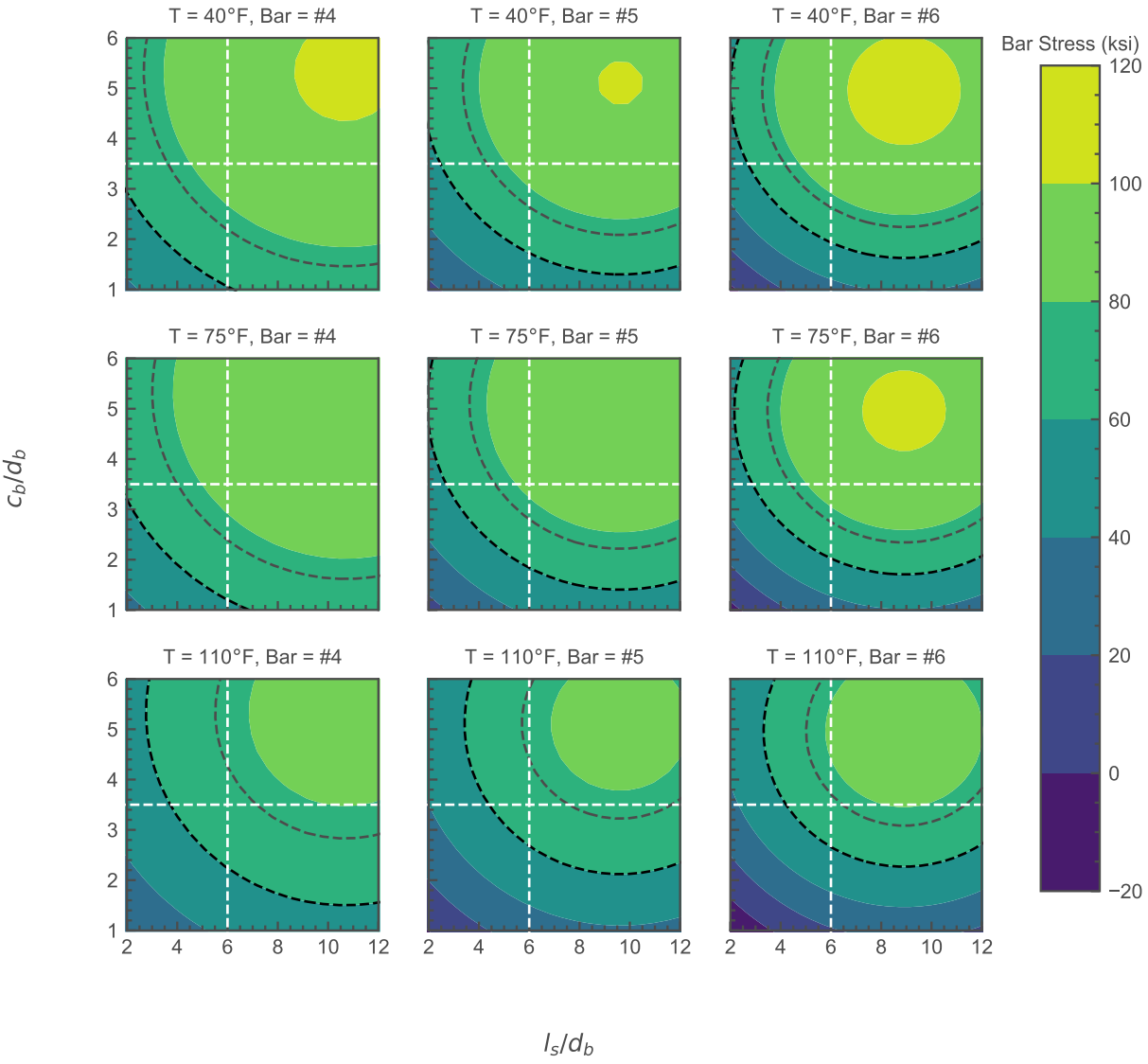

Figure 6-3. Bar stress for varying temperatures and bar sizes

Based on the results of the mechanical properties tested, the material and therefore bond strength of HCSC varies with temperature. However, when used in a closure joint the relative volume of HCSC with respect to cementitious concrete is small. The large volume and thermal mass of concrete would help stabilize and reduce the temperature range of the PC. A conservative temperature was selected for the design recommendation, though additional adjustments should be made based on the known service temperatures of the project location. For the bar sizes and

temperatures shown, the design space specified by the FHWA is sufficient for bar yield at the most conservative edge (110 °F and #6 bars).

At low temperatures, minimal splice length is required to yield the reinforcement, as seen in the top row of Figure 6-3. Additionally smaller bars can have a slightly reduced splice length compared to larger bars, as shown in the left column of the figure. In order to be sufficient for a wider range of temperatures, it is recommended that HCSC follow the recommendations provided by Graybeal (2014) that are adopted in the AASHTO LRFD Guide Specifications for Accelerated Bridge Construction for UHPC. The capability of HCSC to have the same joint geometry efficiency as UHPC helps increase the potential options for a given ABC project.

The closure joint specification recommendations provided by Graybeal are unfactored and are based on the splice length required to yield a Grade 60, epoxy-coated bar at minimum. Additionally, research by Peruchini et al. 2017 concluded that simulated deck specimens had a connection strength of 85.6% of the spliced-connection bond curbs with the same cover and embedment length. The change in bond strength from non-contact splice testing to a service design level model may need to be incorporated into the joint width and reinforcement design.

The use of primers aid in the adhesion of HCSC and other PCs to the adjoining elements and reinforcement. From the scoping study completed, the use of an HMWM primer increases bond by an average of 9%. Joint width and geometry designs should include the use of primer to create a more efficient geometry. Proper preparation and application of primer should be used to ensure proper bond behavior.

The preparation of the bond line surface and reinforcement is critical to ensure good bond between the closure joint material and the precast element. HCSC and other PCs have excellent bond to

itself, reinforcement, and conventional cementitious concrete at connection interfaces with sufficient surface preparation. Good bonding has been shown at interfaces with an exposed aggregate finish. The exposed aggregate finish can be created by applying a retarder to the formwork when casting the precast segments. After form removal, the unhydrated paste can be washed, brushed, or blast off, exposing a rough aggregate surface. Alternatively, abrasive blasting can be used to remove contaminants, open pore structure, and expose aggregate. It is recommended that for closure joints a roughed surface with current best practices be used to provide an exposed aggregate finish.

For closure joints between precast girders, the splice length should account for any sweep that may occur in the structure. The minimal splice length over the length of the closure joint should be ensured in designs and that adequate edge cover be maintained. For closure joints in precast deck panels or precast girders without additional deck overlay, minimum side cover requirements should account for any cross slope or camber of the element.

CHAPTER 7. SUMMARY, CONCLUSIONS, AND RECOMMENDATIONS

7.1. SUMMARY

The use of FRPC as a closure joint material in ABC applications was evaluated as a potential alternative to conventional cementitious concrete and UHPC.

The mechanical properties of HCSC were investigated to determine the effects of temperature and strength gain over time. Three different properties were studied: compressive strength, modulus of rupture, and bond pullout strength. Six batches were mixed, cast, and tested – two batches per property, one for temperature effects and one for early strength gain. For temperature effects, specimens were cast and cured at ambient temperatures and then conditioned to four different testing temperatures, spanning the range of service temperatures in western Washington. To capture the effects of early strength gain, specimens were mixed and cast then tested at early and frequent intervals, starting at two hours after mixing through seven days.

Based on the results of the mechanical characterization, splice length, side cover, bar size, and temperature were chosen as parameters, and their ranges were selected for non-contact splice testing. First, a single batch of non-contact splice specimens was tested to determine the effect of the HMWM primer on the bar stress at failure. After demonstrating the benefits that the HMWM primer had on bond strength, three blocks of ten specimens apiece were cast with parameters (test temperature, T; splice length, ℓ_s; side cover, c_b; and bar diameter, d_b) ranging based on the central composite rotatable experimental design.

Using the collected data, the relationship between the maximum bar stress and splice length, side cover, bar size, and test temperature was estimated by fitting a regression surface. This allowed

the isolation of the individual effects of each parameter. Using these insights, a closure joint width and reinforcement development recommendations were made for the use of HCSC as a closure joint material.

7.2. CONCLUSIONS

The following conclusions were drawn from the study:

- FRPC exhibits significant variation in mechanical properties with temperature. For HCSC, a temperature increase of 40 °F resulted in a roughly 25% reduction in material strength, which was consistent between the compression, flexure, and bond tests. The opposite was true for decreases in temperature.
- There is a tradeoff between working time and the rate of strength development for HCSC. If shorter working times can be tolerated, significant strength (70% of the 7-day value) can be achieved within 2 hours after mixing.
- The development of early compressive, flexure, and bond strengths were very similar. For the level of accelerator used in this study (3% by volume initiator), the compressive, flexural, and bond strengths were roughly 70%, 80%, and 75% of their 7-day values, respectively, 4 hours after mixing.
- For non-contact lap splices embedded in HCSC, the use of HMWM primer increased the bar stress at failure by roughly 9%. The same general trends on the influence of temperature, splice length, and side cover were similar between specimens with and without HMWM primer.

- In non-contact splice specimens, increases in splice length and side cover result in increases in bar stresses at failure. The testing temperature has the opposite effect, with bar stress decreasing as temperature increases.
- Based on RSM analysis of the results of the non-contact splice testing, the AASHTO recommendations for closure joint geometry for UHPC are also applicable for HCSC up to temperatures of 110 °F. Above 110F, additional splice length or bar cover would be required to ensure bar yield before material failure.

7.3. RECOMMENDATIONS FOR FURTHER RESEARCH

Service and Ultimate level joint testing at various temperatures

Small-scale non-contact splice tests were used to isolate the effects of different parameters on bond strength to create a potential joint configuration. Full-scale strength and fatigue testing using sample joint configurations and design recommendations should be completed to validate the behavior of FRPC bond in field scale geometries at different temperatures.

Creep

There is a dearth of research towards understanding the long-term creep characteristics of PCs, although it is well understood that most polymers exhibit significant creep deformations under sustained loads (Hsu 1984). The knowledge of the creep behavior of PCs, like HCSC, is important to understand how the long-term loading affects the overall structure. Creep deformations at joints between precast elements may lead to redistribution of forces within the structure, which may not have been accounted for in design. There are also potential opportunities to leverage the unique time-dependent properties of PC to solve current issues in bridge design. For both of these reasons, the creep characteristics of PCs should be further studied.

REFERENCES

Abdel-Fattah, H., and M. M. El-Hawary. 1999. “Flexural behavior of polymer concrete.” Construction and Building Materials, 13 (5): 253–262. https://doi.org/10.1016/S0950-0618(99)00030-6.

Abokifa, M., and M. A. Moustafa. 2021. “Experimental behavior of poly methyl methacrylate polymer concrete for bridge deck bulb tee girders longitudinal field joints.” Construction and Building Materials, 270: 121840. https://doi.org/10.1016/j.conbuildmat.2020.121840.

Aboutaha, R. S., E. M. Lui, G. Martin, P. Petrina, L. Phoenix, and E. Giannelis. 2005. “Investigation of Durability of Wearing Surfaces for FRP Bridge Decks.” 397.

ACI. 2019. Polymer Concrete: Guidelines for Structural Applications (ACI 548.6R-19). Farmington Hills, MI, USA: Committee 548, American Concrete Institute.

Al-Negheimish, A. I. 1988. “Bond strength, long term performance and temperature induced stresses in polymer concrete-portland cement concrete composite members.”

American Association of State and Highway Transportation Officials. 2012. AASHTO LRFD Bridge Design Specifications. Washington, DC: AASHTO.

American Association of State Highway and Transportation Officials. 2018. AASHTO LRFD guide specifications for accelerated bridge construction. Washington, DC. AASHTO

Anderson, K., M. Russell, K. Littleton, D. McKernan, J. Uhlmeyer, J. Weston, and C. Simonson. 2013. Polyester Polymer Concrete Overlay. Tumwater, WA: Washington State Department of Transportation.

ASTM. 2019. A775/A775M - Standard Specification for Epoxy-Coated Steel Reinforcing Bars. West Conshohocken, PA: ASTM International.

ASTM. 2020a. D7913/D7913M - Standard Test Method for Bond Strength of Fiber-Reinforced Polymer Matrix Composite Bars to Concrete by Pullout Testing. West Conshohocken, PA: ASTM International.

ASTM. 2020b. A370 - Standard Test Methods and Definitions for Mechanical Testing of Steel Products. West Conshohocken, PA: ASTM International.

ASTM. 2021a. C39/C39M - Standard Test Method for Compressive Strength of Cylindrical Concrete Specimens. West Conshohocken, PA: ASTM International.

ASTM. 2021b. C78/C78M - Standard Test Method for Flexural Strength of Concrete (Using Simple Beam with Third-Point Loading). West Conshohocken, PA: ASTM International.

ASTM. 2022. A706/A706M Specification for Deformed and Plain Low-Alloy Steel Bars for Concrete Reinforcement. West Conshohocken, PA: ASTM International.

Box, G. E. P., J. S. Hunter, and W. G. Hunter. 2005. Statistics for experimenters: design, innovation, and discovery. Wiley series in probability and statistics. Hoboken, N.J: Wiley-Interscience.

Carreira, D. J., and K.-H. Chu. 1985. “Stress-Strain Relationship for Plain Concrete in Compression.” JP, 82 (6). https://doi.org/10.14359/10390.

Fowler, D. W. 1999. “Polymers in concrete: a vision for the 21st century q.” 4.

Fowler, D. W., A. H. Meyer, and D. R. Paul. 1981. “Techniques to Improve Strength of Polymer Concrete Made with Wet Aggregate.” 16.

Fowler, D. W., and D. W. Whitney. 2012. Long-Term Performance of Polymer Concrete for Bridge Decks. 14623. Washington, D.C.: National Cooperative Highway Research Program.

Garber, D., and E. Shahrokhinasab. 2019. “ABC-UTC Guide for: Full-Depth Precast Concrete (FDPC) Deck Panels.”

Graybeal, B. 2014. Bond Behavior of Reinforcing Steel in Ultra-High Performance Concrete. Washington, D.C.: USDOT FHWA.

Graybeal, B. A. 2006. Material Property Characterization of Ultra-High Performance Concrete. 188. Washington, D.C.: USDOT FHWA.

Guedes, R. M., C. M. L. Tavares, and A. J. M. Ferreira. 2004. “Experimental and theoretical study of the creep behavior of GFRP-reinforced polymer concrete.” Composites Science and Technology, 64 (9): 1251–1259. https://doi.org/10.1016/j.compscitech.2003.10.004.

Haber, Z. B., and B. A. Graybeal. 2018. “Lap-Spliced Rebar Connections with UHPC Closures.” J. Bridge Eng., 23 (6): 04018028. https://doi.org/10.1061/(ASCE)BE.1943-5592.0001239.

Haber, Z. B., I. D. la Varga, B. A. Graybeal, Brian Nakashoji, and Rafic El-Helou. 2018. Properties and Behavior of UHPC-Class Materials. Washington, D.C.: USDOT FHWA.

Hassani Niaki, M., A. Fereidoon, and M. Ghorbanzadeh Ahangari. 2018. “Experimental study on the mechanical and thermal properties of basalt fiber and nanoclay reinforced polymer concrete.” Composite Structures, 191: 231–238. https://doi.org/10.1016/j.compstruct.2018.02.063.

Heidari-Rarani, M., M. R. M. Aliha, M. M. Shokrieh, and M. R. Ayatollahi. 2014. “Mechanical durability of an optimized polymer concrete under various thermal cyclic loadings – An experimental study.” Construction and Building Materials, 64: 308–315. https://doi.org/10.1016/j.conbuildmat.2014.04.031.

Hong, S. 2017. “Influence of Curing Conditions on the Strength Properties of Polysulfide Polymer Concrete.” Applied Sciences, 7 (8): 833. https://doi.org/10.3390/app7080833.

Hsu, H.-T. 1984. “Flexural Behavior of Polymer Concrete Beams.” Austin, Texas: The University of Texas of Austin.

Hsu, M., and D. W. Fowler. 1985. “Creep and Fatigue of Polymer Concrete.” ACI Symposium Publication, 89. https://doi.org/10.14359/6256.

Krauss, P. D., and J. S. Lawler. 2018. Bond Behavior of Reinforcing Steel in Kwik Bond Polyester Polymer Concrete. 24. Northbrook, IL: Wiss, Janney, Elstner Associates, Inc.

Kwik Bond Polymers. 2020b. “Product Data Sheet: Hybrid Composite Synthetic Concrete (HCSC).”

Kwik Bond Polymers. 2020a. “Product Data Sheet: PPC 1121 Polyester Polymer Concrete.”

Maas, J. 1997. “I-80—It’s Almost a Decade.” In-Place Performance of Polymer Concrete Overlays, SP-169, 172–179. Farmington Hills, MI: American Concrete Institute.

Maas, J. 2003. “How Polyester Polymer Concrete Highway and Bridge Deck Overlays Became ‘State of the Art.’” Polymers in Concrete: The First Thirty Years, SP-214, 39–49. Farmington Hills, MI: American Concrete Institute.

Mantawy, I., R. Chennareddy, M. Genedy, and M. R. Taha. 2019. “Polymer Concrete for Bridge Deck Closure Joints in Accelerated Bridge Construction.” Infrastructures, 4 (2): 31. https://doi.org/10.3390/infrastructures4020031.

Mebarkia, S., and C. Vipulanandan. 1992. “Compressive Behavior of Glass-Fiber Reinforced Polymer Concrete.” Journal of Materials in Civil Engineering, 4 (1): 91–105. https://doi.org/10.1061/(ASCE)0899-1561(1992)4:1(91).

Minitab. 2022. “Getting Started with Minitab Statistical Software.”

Moustafa, M., A. Itani, and M. Abokifa. 2019. “More Choices for Connecting Prefabricated Bridge Deck Elements.” Reno, NV.

Oussama, E., G. Elhem, V. Mignot, and B. O. Mongi. 2012. “Mechanical and physical properties of epoxy polymer concrete after exposure to temperatures up to 250°C.” Construction and Building Materials, 27 (1): 415–424. https://doi.org/10.1016/j.conbuildmat.2011.07.027.

Park, S.-K., B.-W. Jo, D.-H. Park, and B.-S. Chun. 2010. “Flexural rigidity and ductility of high-strength reinforced polyester polymer concrete beams.” Advances in Cement Research, 22 (2): 91–97. https://doi.org/10.1680/adcr.2010.22.2.91.

Peruchini, T. J. 2017. “Investigation of Ultra-High Performance Concrete for Longitudinal Joints in Deck Bulb Tee.” University of Washington.

Peruchini, T. J., J. Stanton, and P. Calvi. 2017. Investigation of Ultra-High Performance Concrete for Longitudinal Joints in Deck Bulb Tee Bridge Girders. 213. Olympia, WA: Washington State Department of Transportation.

Poillucci, R. A., and C. Hansen. 2013. “Reducing use of styrene monomer in unsaturated polyester resins.” 23.

Qiao, P., Z. Zhidong, and S. Allena. 2016. Developing Connections for Longitudinal Joints between Deck Bulb Tees -- Development of UHPC Mixes with Local Materials. 119. Olympia, WA: Washington State Department of Transportation.

Reis, J. 2005. “Mechanical characterization of fiber reinforced Polymer Concrete.” Mat. Res., 8 (3): 357–360. https://doi.org/10.1590/S1516-14392005000300023.

Reis, J. M. L., and A. J. M. Ferreira. 2006. “Freeze–thaw and thermal degradation influence on the fracture properties of carbon and glass fiber reinforced polymer concrete.”

Construction and Building Materials, 20 (10): 888–892. https://doi.org/10.1016/j.conbuildmat.2005.06.021.

Ribeiro, M. C. S., P. R. Nóvoa, A. J. M. Ferreira, and A. T. Marques. 2004. "Flexural performance of polyester and epoxy polymer mortars under severe thermal conditions." Cement and Concrete Composites, 26 (7): 803–809. https://doi.org/10.1016/S0958-9465(03)00162-8.

Ribeiro, M. C. S., J. M. L. Reis, A. J. M. Ferreira, and A. T. Marques. 2003a. "Thermal expansion of epoxy and polyester polymer mortars—plain mortars and fibre-reinforced mortars." Polymer Testing, 22 (8): 849–857. https://doi.org/10.1016/S0142-9418(03)00021-7.

Ribeiro, M. C. S., C. M. L. Tavares, M. Figueiredo, A. J. M. Ferreira, and A. A. Fernandes. 2003b. "Bending characteristics of resin concretes." Mat. Res., 6 (2): 247–254. https://doi.org/10.1590/S1516-14392003000200021.

Sett, K., and C. Vipulanandan. 2004. "Properties of Polyester Polymer Concrete with Glass and Carbon Fibers." ACI Materials Journal, 101 (1). https://doi.org/10.14359/12985.

Shahrokhinasab, E., and D. Garber. 2021. Development of "ABC-UTC Non-Proprietary UHPC" Mix. FIU.

Sika. 2020. "Product Data Sheet: Sikadur-25 Lo-Mod EPU."

Sprinkel, M. 1997. "Nineteen Year Performance of Polymer Concrete Bridge." ACI Symposium Publication, 169. https://doi.org/10.14359/5930.

Sprinkel, M. 2003. "Twenty-Five-Year Experience with Polymer Concrete Bridge Deck Overlays." ACI Symposium Publication, 214. https://doi.org/10.14359/12760.

Stevens, R. J., and W. S. Guthrie. 2021. “Scanning Tour of Polyester Polymer Concrete Overlays on Bridge Decks in California.” Tran-SET 2020, 287–297. Albuquerque, New Mexico (Conference Held Virtually): American Society of Civil Engineers.

Toufigh, V., M. Hosseinali, and S. M. Shirkhorshidi. 2016. “Experimental study and constitutive modeling of polymer concrete’s behavior in compression.” Construction and Building Materials, 112: 183–190. https://doi.org/10.1016/j.conbuildmat.2016.02.100.

Transpo Industries, Inc. n.d. “Product Data Sheet: T-17 Rapid Patch.”

Vipulanandan, C., and S. Mebarkia. 1996. “Flexural and Facture Properties of Glass Fiber Reinforced Polyester Polymer Concrete.” ACI Symposium Publication, 166. https://doi.org/10.14359/1394.

Vipulanandan, C., and E. Paul. 1990. “Performance of Epoxy and Polyester Polymer Concrete.” ACI Materials Journal, 87 (3). https://doi.org/10.14359/2187.

Wagner, E. 2021. Kwik Bond Hybrid Composite Synthetic Concrete (HCSC) Material Characterization. 11. Northbrook, IL: Wiss, Janney, Elstner Associates, Inc.

Wagner, E. I., and P. D. Krauss. 2020. Bond Behavior of Reinforcing Steel in Kwik Bond HCSC Material. 15. Northbrook, IL: Wiss, Janney, Elstner Associates, Inc.

Yuan, J., and B. Graybeal. 2014. Bond Behavior of Reinforcing Steel in Ultra-High Performance Concrete. 78. Washington, D.C.: USDOT FHWA.